Bulletin of the Seismological Society of America, Vol. 93, No. 1, pp. 332–352, February 2003

Amplification Factors for Spectral Acceleration in Tectonically Active Regions

by Jonathan P. Stewart, Andrew H. Liu, and Yoojoong Choi

Abstract Empirical relationships are developed to predict amplification factors for 5% damped response spectral acceleration (period range T = 0.01–5 sec) as a function of site category. We evaluate amplification factors by normalizing response spectral accelerations computed from recordings by reference spectral accelerations derived from a modified attenuation relationship for active regions. Strong motion sites are categorized according to several schemes, which are based on surface geology (age-only, age + depositional environment, and age + material texture), shallow (30 m) shear-wave velocity, and geotechnical data. Criteria for selection of the optimal classification scheme are that the amplification models for categories within the scheme (1) minimize the global dispersion of prediction residuals and (2) are significantly distinct across a broad period range. The results of the regressions indicate that the greatest levels of distinction in amplification levels across categories occur for the shallow shear-wave velocity scheme, but that the dispersion of residuals for this scheme are relatively high for soil sites (although not for rock sites). Conversely, schemes based on detailed surface geology generally have the smallest dispersion for soil sites, but amplification levels across Quaternary categories are only significantly distinct at small periods. These findings suggest that detailed surface geology provides an effective means of soil site categorization at small periods, whereas shallow shear-wave velocity provides an effective means for rock site categorization at small periods. At longer periods, none of the schemes are optimized relative to both the *dispersion* and *distinction* criteria. The principal application of the amplification factors is as a modifier of attenuation relations (much like a site term). The present results significantly reduce the bias associated with the site terms in a widely used attenuation relationship for rock and soft soil site conditions.

Introduction

Ground-motion attenuation relationships are used in seismic hazard analyses to provide a probabilistic distribution of a particular ground-motion intensity measure (IM), such as 5% damped response spectral acceleration, conditional on magnitude, site-source distance, and parameters representing site condition and style-of-faulting. Ground-motion data are often log-normally distributed, in which case the distribution can be represented by a median and standard deviation, σ (in natural logarithmic units). Site condition is often characterized in attenuation relations as either rock or soil. Actual conditions at strong motion recording sites are variable with respect to local site conditions and underlying basin structure, and hence estimates from attenuation relationships necessarily represent averaged values across the range of possible site conditions within the *rock* or *soil* categories. Ground-motion amplification factors provide a means by which more detailed information on site conditions can be used to improve ground motion predictions relative to what is obtained with attenuation relationships. This "improvement" in ground-motion prediction generally involves (1) removing potential bias in median ground-motion estimates that might be present for a particular site condition, and (2) reducing the uncertainty in ground-motion estimates, as measured by standard error term, σ.

Amplification factors represent the ratio of an observed IM to a reference value of that IM for a particular site condition (e.g., intact rock or rock-average for active regions). Since ground-motion recordings are affected by source, path, and site effects, the evaluation of amplification factors from recorded motions requires the removal of source and path effects. This can be accomplished by comparing, for a given earthquake, IMs from sites with various geologic conditions to IMs from *reference* (usually firm rock) sites, with appropriate corrections for distance variations between the sites. A number of variations on this so-called reference site approach are described by Field and Jacob (1995), and the

approach has been widely used (e.g., Boatwright *et al.*, 1991; Borcherdt and Glassmoyer, 1994; Harmsen, 1997; Borcherdt, 2002; Hartzell *et al.*, 2000).

The second category of approaches for evaluating site amplification effects does not require the presence of a reference site. Field and Jacob (1995) review several variations on non-reference site approaches. We adopt a non-reference site approach in which amplification is evaluated by normalizing the spectra of recorded motions by a reference (rock) spectrum obtained from an attenuation relationship. This approach has been applied to specific basins by Sokolov (1997) and Sokolov *et al.* (2000) using locally derived attenuation functions for Fourier amplitude spectra and for the southern California region using attenuation relations for spectral acceleration (Field, 2000; Lee and Anderson, 2000; Steidl, 2000). Two significant advantages to this approach include: (1) relatively large amounts of strong motion data can be utilized, and (2) amplification factors derived from attenuation residuals can be readily incorporated into conventional hazard analyses (i.e., the amplification factors provide straightforward modifications to the median and standard error from attenuation relations).

The objectives of our study are (1) to develop empirical amplification factors for 5% damped response spectral acceleration (period range T = 0.01-5 sec) using a comprehensive strong motion database for active regions, (2) to classify the strong motion stations based on geologic and geotechnical classification schemes using recently developed data resources not available to previous investigators, and (3) to investigate the relative effectiveness of various site classification schemes in terms of their ability to minimize IM dispersion levels and to delineate distinct amplification levels between categories. The relatively large size of the strong motion database and the opportunity to compare results for various alternative site classification schemes represent significant new features of the present study. The results are considered applicable to active tectonic regions (i.e., areas near plate boundaries but from non-subduction earthquakes) because the data used in the study are derived from such regions/earthquakes. It is possible that the amplification factors derived from these data are also applicable to other tectonic regimes, although this should be verified with data in future studies.

We begin by describing the site classification schemes used in the study and our strong motion/borehole databases. We should note that the classification schemes considered herein are all based on characteristics of near-surface geologic materials, that is, the effects of deep basin structure are not considered. We then describe the processes used to interpret the data through the example of a relatively simple, age-based geologic classification scheme. Included in the interpretation are statistical tests for the nonlinearity of amplification factors and the level of distinction between site categories. We then review the results for each classification scheme, and identify the classification schemes that minimize the dispersion of prediction residuals. The cumulative results of the study provide insight into the "optimal" classification schemes for defining empirical amplification factors (with the constraint that the schemes are all based on characteristics of near-surface materials). Recommendations for practical application of the amplification factors are also provided.

Databases

Strong-Motion Data

The ground motion database used in this study consists of 1828 recordings from 154 earthquakes. These recordings are from worldwide shallow crustal earthquakes near active plate margins. Subduction and inter-plate events are excluded. Event dates range from the 1933 Long Beach, California earthquake to the 1999 Duzce, Turkey earthquake. Removed from the data set for this study were recordings from events with poorly defined magnitude or focal mechanism, recordings for which site-source distances are poorly constrained because of the lack of a finite source model, and recordings for which problems were detected with one or more components. These removals reduced the data set to 1032 recordings from 51 events, which are distributed in magnitude–distance space as shown in Figure 1. Characteristics of the events are listed in Table 1, which shows that the events are principally from California, Turkey, and Japan. Note that the attenuation with distance observed during the recent Turkey earthquakes and the Kobe, Japan earthquake was found to be similar to that predicted by attenuation relations derived principally from California recordings (EERC, 1995; Rathje *et al.*, 2000), which justifies the use of those data in this study. Data from the 1999 Chi-Chi, Taiwan

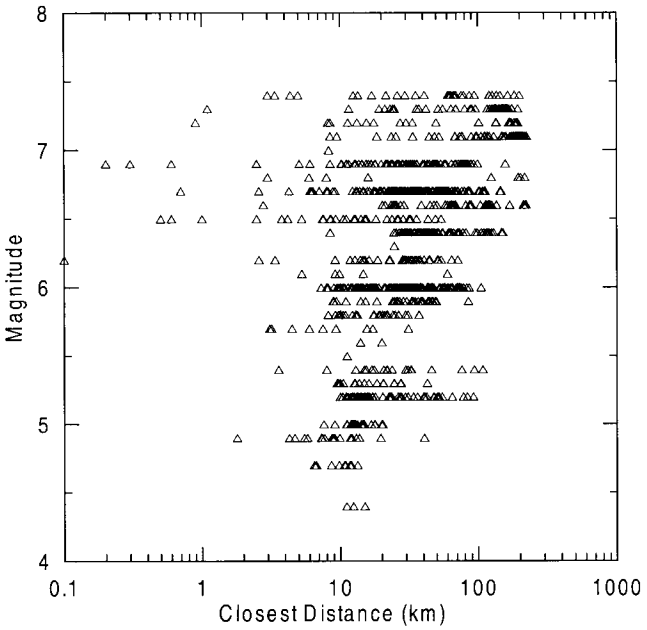

Figure 1. Inventory of strong motion recordings utilized in this study.

Table 1
Earthquakes Used in this Study

Event	Year	Mo-Day	Time	Magnitude
Imperial Valley	1940	5-19	437	7.0
Kern County	1952	7-21	1153	7.4
San Francisco	1957	3-22	1944	5.3
Parkfield	1966	6-28	426	6.1
Borrego Mtn	1968	4-09	230	6.8
Lytle Creek	1970	9-12	1430	5.4
Hollister	1974	11-28	2301	5.2
Oroville	1975	8-01	2020	6.0
Oroville	1975	8-02	2022	5.0
Oroville	1975	8-02	2059	4.4
Oroville	1975	8-08	700	4.7
Santa Barbara	1978	8-13		6.0
Tabas, Iran	1978	9-16		7.4
Coyote Lake	1979	8-06	1705	5.7
Imperial Valley	1979	10-15	2316	6.5
Imperial Valley	1979	10-15	2319	5.2
Imperial Valley	1979	10-16	658	5.5
Livermore	1980	1-24	1900	5.8
Livermore	1980	1-27	233	5.4
Mammoth Lakes	1980	5-27	1901	4.9
Mammoth Lakes	1980	5-31	1516	4.9
Mammoth Lakes	1980	6-11	441	5.0
Westmoreland	1981	4-26	1209	5.8
Coalinga	1983	5-02	2342	6.4
Coalinga	1983	5-09	249	5.0
Coalinga	1983	6-11	309	5.3
Coalinga	1983	7-09	740	5.2
Coalinga	1983	7-22	239	5.8
Morgan Hill	1984	4-24	2115	6.2
Bishop (Rnd Val)	1984	11-23	1912	5.8
Hollister	1986	1-26	1920	5.4
N. Palm Springs	1986	7-08	920	6.0
Chalfant Valley	1986	7-20	1429	5.9
Chalfant Valley	1986	7-21	1442	6.2
Chalfant Valley	1986	7-21	1451	5.6
Chalfant Valley	1986	7-31	722	5.8
Whittier Narrows	1987	10-01	1442	6.0
Whittier Narrows	1987	10-04	1059	5.3
Superstition Hills (A)	1987	11-24	514	6.3
Superstition Hills (B)	1987	11-24	1316	6.7
Loma Prieta	1989	10-18	5	6.9
Cape Mendocino	1992	4-25	1806	7.1
Landers	1992	6-28	1158	7.3
Big Bear	1992	6-28	1506	6.4
Northridge	1994	1-17	1231	6.7
Northridge Aftershock	1994	1-17	431	5.9
Northridge Aftershock	1994	3-20	1320	5.2
Kobe, Japan	1995	1-16	2046	6.9
Kocaeli, Turkey	1999	8-17		7.4
Hector Mine	1999	10-16	946	7.1
Duzce, Turkey	1999	11-12		7.2

earthquake were not used due to the preliminary nature of the site classifications (Lee *et al.*, 2001).

The ground-motion intensity measure for which amplification factors are derived in this study is 5% damped response spectral acceleration (S_a). The spectral periods considered range from T = 0.01 to 5 sec. However, spectral ordinates with frequencies less than $f = 1.25 \times f_{HP}$ are not used, where f_{HP} = high-pass frequency used during data processing. We do not discard ordinates at frequencies higher than the low-pass frequency (f_{LP}) because of the saturation of S_a at high frequency.

Sources of strong motion data for the western United States include the California Strong Motion Instrumentation Program (CSMIP), the U.S. Geological Survey (USGS), the University of Southern California (USC), the California Division of Mines and Geology (CDMG), and the Los Angeles Department of Water and Power (LADWP). Additional data have been obtained for the 1999 Kocaeli and Duzce, Turkey, earthquakes from the Kandilli Observatory and Earthquake Engineering Research Institute of Boğaçizi University (Kandilli), the Earthquake Research Department of the General Directorate of Disaster Affairs (ERD), and Istanbul Technical University (ITU). Most of the time histories used in this study can be obtained at the web site of the Pacific Earthquake Engineering Research Center (www.peer.berkeley.edu). All data were decimated to a common time step of 0.02 sec by first low-pass filtering the data with a corner frequency of 25 Hz (using an eighth-order Chebyshev type-I filter), and then resampling the resulting signal at the time step of 0.02 sec. Otherwise, the time signals were unaltered.

The distance measure used here is the closest distance to the rupture plane, which can include a vertical component for dipping source zones and buried strike-slip source zones. Magnitude is taken as moment magnitude where available and is otherwise taken as surface-wave magnitude for $M > 6$ and local magnitude for $M < 6$.

Site Classifications

Surface Geology. A total of 427 California recording stations were classified based on mapped surface geology for use in this study. A complete listing of these classifications, and the references used for each site, is provided in Stewart *et al.* (2001). Additional (non-California) sites include 21 stations near Kobe, Japan (classified by Fukushima *et al.*, 2000), 8 stations near Tabas, Iran (classified by Shoja-Taheri and Anderson, 1978), 7 stations in northern Mexico (classified by Geomatrix, 1993), and 30 stations in Turkey (classified in this study). Attempts were made to classify each site according to the three geologic classification schemes shown in Table 2, which are based on geologic age-only (493 classified sites, 900 motions), age + depositional environment (259 sites, 495 motions), and age + material texture (179 sites, 334 motions).

Geologic classifications for California strong motion stations were developed using sources with variable levels of detail. The geology of the entire state is documented on 27 maps at 1:250,000 scale by the California Division of Mines and Geology (CDMG, 1959–1998). These maps distinguish Quaternary deposits based on age (Holocene–Pleistocene) and generalized descriptions of depositional environment. The Southern California Aerial Mapping Project

Table 2
Criteria for Surface Geology Classifications*

Age	Depositional Environment	Sediment Texture
Holocene (286)	Holocene alluvium (159)	Holocene Coarse (70)
Pleistocene (88)	Pleistocene alluvium (37)	Pleistocene Coarse (19)
	H. lacustrine/marine (36)	Holo. Fine-Mixed (72)
	P. lacustrine/marine (9)	Pleist. Fine-Mixed (18)
	Aeolian (6)	
	Artificial Fill (12)	
Tertiary (59)		
Mesozoic + Igneous (60)		

* Number of sites indicated in parentheses

Table 3
Site Categories in NEHRP Provisions (Martin, 1994)

NEHRP Category	Description	Mean Shear Wave Velocity to 30 m
A	Hard Rock	> 1500 m/sec
B	Firm to hard rock	760–1500 m/sec
C	Dense soil, soft rock	360–760 m/sec
D	Stiff soil	180–360 m/sec
E	Soft clays	< 180 m/sec
F	Special study soils, e.g., liquefiable soils, sensitive clays, organic soils, soft clays > 36 m thick	

(SCAMP) is compiling more detailed geologic information for selected quadrangles in southern California. For example, data for the Santa Ana 30′ × 60′ quadrangle have been prepared at 1:100,000 scale by Morton *et al.* (1999) and were used in this study. In addition, we used digital geologic maps at 1:24,000 scale prepared through SCAMP of 7.5′ quadrangles in Los Angeles and Orange counties (CDMG staff, personal comm., 2000). The SCAMP maps are the most detailed of the available geologic maps, providing basic information on the texture of Quaternary deposits (e.g., coarse/fine/mixed) and detailed information on depositional environment.

Near-Surface Shear-Wave Velocity. The average shear-wave velocity of shallow sediments is commonly represented by parameter $V_{s\text{-}30}$, which is calculated as the ratio of 30 m to the vertical shear wave travel time through the upper 30 m of the site. Based on empirical studies by Borcherdt and Glassmoyer (1994), Borcherdt (1994) recommended $V_{s\text{-}30}$ as a means of classifying sites for building codes, and similar site categories were selected for the National Earthquake Hazards Reduction Program (NEHRP) seismic design provisions for new buildings (Martin, 1994). The $V_{s\text{-}30}$-based site classification scheme in the NEHRP provisions is presented in Table 3. An exception to the $V_{s\text{-}30}$ criteria is made for soft clays (defined as having undrained shear strength <24 kPa, plasticity index >20, and water content >40%), for which category E is assigned if the thickness of soft clay exceeds 3 m regardless of $V_{s\text{-}30}$.

It should be noted that shear-wave velocity has been found to be well correlated to detailed surface geology (age + texture for soil, age + weathering/fracture spacing for rock) by Fumal (1978). The $V_{s\text{-}30}$ parameter has been correlated with surface geology by Wills and Silva (1998), and this information has been used to generate state-wide maps of $V_{s\text{-}30}$ by Wills *et al.* (2000).

To classify strong motion sites according to the $V_{s\text{-}30}$ parameter, a GIS database was developed having the locations of both strong motion stations and boreholes in California. Each strong motion station location was checked with instrument owners (USGS and CSMIP) or against published reports (USC—Anderson *et al.*, 1981), to optimize accuracy. Borehole locations were generally obtained from maps in reports. The borehole database is similar to that of Wills and Silva (1998) but also contains additional Caltrans boreholes, boreholes from selected consulting geotechnical engineers, and data recently compiled in the ROSRINE program (*http://geoinfo.usc.edu/rosrine/*). These databases were used to match boreholes with strong motion sites if (1) both locations are on the same surface geology, and (2) the separation distance was <1600 m.

The above databases were used to pair 228 strong motion stations to boreholes with geophysical measurements. Of these sites, 190 have borehole–accelerograph separation distances <160 m, 13 from 160 to 450 m, and 25 from 450 to 1600 m. The borehole geophysical data was used to develop $V_{s\text{-}30}$ values and NEHRP classifications, which break down as follows: A, 13; B, 17; C, 81; D, 114; E, 13 sites. It should be noted that shear-wave velocities for USC strong motion stations obtained by Rodriguez-Ordonez (1994) were not used due to apparent biases in such data as documented by Boore and Brown (1998) and Wills and Silva (1998). A complete inventory of the classifications is presented in Stewart *et al.* (2001).

Geotechnical Data. Geotechnical engineers have developed site classification schemes that can be used to estimate response spectra for soil sites. Early work on this topic is summarized in Seed and Idriss (1982), who recommended the following site classification scheme:

1. Rock sites
2. Stiff soil sites (<60 m deep)
3. Deep cohesionless soil sites (>75 m deep)
4. Sites underlain by soft to medium stiff clays

Dickenson (1994) and Chang (1996) proposed new site categories based on significant additional data gathered from the 1985 Mexico City, 1989 Loma Prieta, and 1994 Northridge earthquakes. The key feature that differentiates these geotechnical schemes from other schemes discussed previously is the incorporation of information on sediment depth.

The most recent of the geotechnical classification schemes is shown in Table 4, and was proposed by

Table 4
Geotechnical site categories proposed by Rodriguez-Marek et al. (2001)

Site	Description	Comments
A	Hard Rock	Crystalline Bedrock; $V_s \geq 1500$ m/sec
B	Competent Bedrock	$V_s \geq 600$ m/sec or <6 m of soil. Most "unweathered" California Rock cases
C1	Weathered Rock	$V_s \sim 300$ m/sec increasing to >600 m/sec, weathering zone > 6 m and < 30 m
C2	Shallow Stiff Soil	Soil depth > 6 m and < 30 m
C3	Intermediate Depth Stiff Soil	Soil depth > 30 m and < 60 m
D1	Deep Stiff Holocene Soil	Depth > 60 m and < 200 m
D2	Deep Stiff Pleistocene Soil	Depth > 60 m and < 200 m
D3	Very Deep Stiff Soil	Depth > 200 m
E1	Medium Thickness Soft Clay	Thickness of soft clay layer 3–12 m
E2	Deep Soft Clay	Thickness of soft clay layer > 12 m
F	Potentially Liquefiable Sand	Holocene loose sand with high water table ($z_w \leq 6$ m)

Rodriguez-Marek *et al.* (2001) based on event-specific regressions of Loma Prieta and Northridge earthquake recordings. Rodriguez-Marek *et al.* (2001) recommend use of their classification scheme over the $V_{s\text{-}30}$ scheme as they found intra-category standard error terms for these two earthquakes to be minimized through the use of the geotechnical scheme.

The effort to match boreholes and strong-motion stations described above was leveraged to develop geotechnical site classifications according to the scheme in Table 4. Details of the process by which geotechnical classifications were assigned to strong motion stations are provided in Stewart *et al.* (2001). The breakdown of sites in the various categories is as follows: A, 1; B, 35; C, 69; D, 90; E, 14 sites.

Data Analysis

Amplification Factors from Individual Recordings

The amplification factor for ground motion j within site category i, F_{ij}, is evaluated from the geometric mean of 5% damped acceleration response spectra for the two horizontal components of shaking, S_{ij}, and the reference ground motion for the site, $(S_r)_{ij}$, as follows:

$$F_{ij}(T) = S_{ij}/(S_r)_{ij} \quad (1)$$

where $T =$ spectral period. In equation (1), S_{ij} and $(S_r)_{ij}$ are computed at the same spectral period, which is varied from 0.01 to 5 sec. Amplification factors are not evaluated for $T > 1/(f_{hp} \times 1.25)$ where f_{hp} is high-pass corner frequency. Reference motion parameter $(S_r)_{ij}$ is taken as the median spectral acceleration calculated from the Abrahamson and Silva (1997) attenuation relationship for rock sites, with modifications for event terms and rupture directivity effects. The rock attenuation estimate is a function of moment magnitude (**M**), closest site-source distance (r), rupture mechanism, and location of the site on or off the hanging wall of dip-slip faults. For well-recorded events, the event term represents the period-dependent average residual between motions from a given event and the general attenuation model. These terms are evaluated during the development of attenuation models with a random effects regression procedure (Abrahamson and Youngs, 1992). The rupture directivity correction is made for sites near the seismic source using the empirical model by Somerville *et al.* (1997), later modified by Abrahamson (2000).

By evaluating reference motion parameters through the use of a rock attenuation relationship, the site condition associated with this reference motion is vaguely defined. This is because many site conditions are present at the recording sites represented within the "rock" category. Some sites have fresh, relatively hard rock, but most consist of deeply weathered, relatively soft rock. The median $V_{s\text{-}30}$ values for these rock sites has been assessed as 520 and 620 m/sec from compilations of borehole geophysical data by Silva *et al.* (1997) and Boore *et al.* (1997), respectively. Ambiguity in the reference site condition can be smaller when amplification factors are derived using reference site approaches (e.g., Borcherdt, 2002). However, for practical purposes, what is most important is that the reference site condition is one for which attenuation relationships can be readily defined, and one for which attenuation estimates of IMs are stable over time (i.e., as more earthquakes are added to the regression data set). Both criteria are satisfied through the approach taken here. First, use of the broad "rock" category provides ample recordings from which attenuation relations have previously been developed. Second, the use of event terms for well-recorded events provide stability because when coupled with the rock attenuation estimate of IMs, event terms for a given event define the rock average for that event, which would not be expected to change significantly over time.

The ground-motion amplification provided by equation (1) is subject to error as a result of the uncertainty associated with reference motion $(S_r)_{ij}$. Because S_{ij} is known, the standard error of the ground-motion amplification for a particular site, $(\sigma_f)_{ij}$, is equivalent to the standard error of the reference motion estimate, $(\sigma_r)_{ij}$, that is,

$$(\sigma_f)_{ij} = (\sigma_r)_{ij}. \quad (2)$$

Standard error terms from attenuation relationships are fairly large ($\sim 0.4 - 0.9$), and hence the uncertainty in individual estimates of amplification is also large. However, the central limit theorem in statistical theory (e.g., Ang and Tang, 1975) suggests that statistical moments (i.e., mean, standard deviation) estimated from large data populations are relatively insensitive to the probability density function associated with individual data points in the population. Accordingly, the errors in point estimates of amplification can be accepted when relations for amplification factors are regressed upon using a large database. As discussed subsequently in the article, confidence intervals around regressed amplification functions are calculated to quantify the degree to which the database is sufficiently large for a particular site category.

Finally, it is acknowledged that the evaluation of amplification factors in terms of response spectral ordinates is less physically based than Fourier amplitude ratios, which have been used in some previous studies. The use of response spectral ratios was prompted by two factors: (1) state-of-the-art procedures for evaluating reference motions in terms of response spectral ordinates are more maturely developed than those for Fourier spectral ordinates, and (2) seismic hazard analyses are typically performed in terms of response spectral ordinates, and hence amplification factors expressed in term of spectral ordinates will have greater practical application.

Regression Procedure

Amplification factors computed using equation (1) were sorted into site categories defined by the schemes in Tables 2–4. For a particular scheme, within a given category i, regression analyses were performed to relate amplification factors, F_{ij}, to ground motion amplitude as follows:

$$\ln(F_{ij}) = a_i + b_i \ln(G_{ij}) + \varepsilon_{ij}, \quad (3a)$$

where a_i and b_i are regression coefficients specific to category i, G_{ij} is a parameter representing the amplitude of the reference ground motion for site j, and ε_{ij} is an error term. This same regression equation has been used by Youngs (1993) and Bazzuro (1998), with G_{ij} taken as the peak horizontal acceleration for the reference site condition (PHA_r). Abrahamson and Silva (1997) also took G_{ij} as PHA_r but added a constant term to G_{ij}:

$$\ln(F_{ij}) = a_i + b_i \ln(G_{ij} + c) + \varepsilon_{ij}, \quad (3b)$$

where $c = 0.03g$ independent of period. This form of the regression equation was also investigated here but was not found to decrease data dispersion, and so the c term was dropped.

We investigated the use of several G_{ij} parameters for evaluating amplification, including PHA_r, spectral acceleration at the same period used in the evaluation of F_{ij}, and peak velocity (calculated using the attenuation relation by Campbell [1997, 2000, 2001]). As reported in Stewart and Liu (2000), G_{ij} parameters other than PHA_r did not reduce data dispersion relative to those for PHA, and so in the following we take G_{ij} as PHA_r.

Due to the incorporation of event terms into the reference motions for spectral acceleration, systematic variations of amplification factors across events are not expected. Accordingly, least-square regression analyses are performed (which give equal weight to all points) in lieu of a random effects model such as that of Abrahamson and Youngs (1992).

Residuals (ε_{ij}) between the amplification "prediction" of equation (3a) and $\ln(F_{ij})$ values were evaluated [$\varepsilon_{ij} = \ln(F_{ij})_{data} - \ln(F_{ij})_{model}$] for all data in category i to enable evaluation of the mean residual, ε_i, and the standard deviation of the residual, σ_i.

$$\varepsilon_i = \frac{1}{N_i} \sum_{j=1}^{N_i} \varepsilon_{ij} \quad (4a)$$

$$\sigma_i = \sqrt{\frac{\sum_{j=1}^{N_i} (\varepsilon_{ij} - \varepsilon_i)^2}{N_i - df_i}}, \quad (4b)$$

where N_i = number of data points in category i and df_i = number of degrees of freedom in regression equation for category i (two in this case). The mean residual is always zero, that is, $\varepsilon_i = 0$. Well-defined site categories would be expected to have smaller values of σ_i than relatively broad categories.

Example Results and Statistical Testing of Results

In this section, we present example results for the age-only geologic classification scheme and describe the statistical tests performed on the data. For each age category, we plot in Figure 2 the spectral amplification at four periods—peak horizontal acceleration (PHA), $T = 0.3$, 1.0, and 3.0 sec. Also plotted are results of regression analyses performed according to equation (3a) (solid lines), ± 95% confidence intervals on the median amplification (dotted lines), and median regression ± standard error, σ (dashed lines). The regression coefficients and standard error terms are listed in Table 5. The estimation error terms for parameters a_i and b_i in Table 5 are the half-widths of the ±95% confidence intervals on the parameters.

Reductions of amplification factors with increasing PHA_r are taken as evidence of sediment nonlinearity. This nonlinearity is quantified by the b_i parameter for each category i. The statistical significance of the PHA_r-dependence of amplification factors is assessed two ways. The first significance test consists of comparing the absolute value of b_i

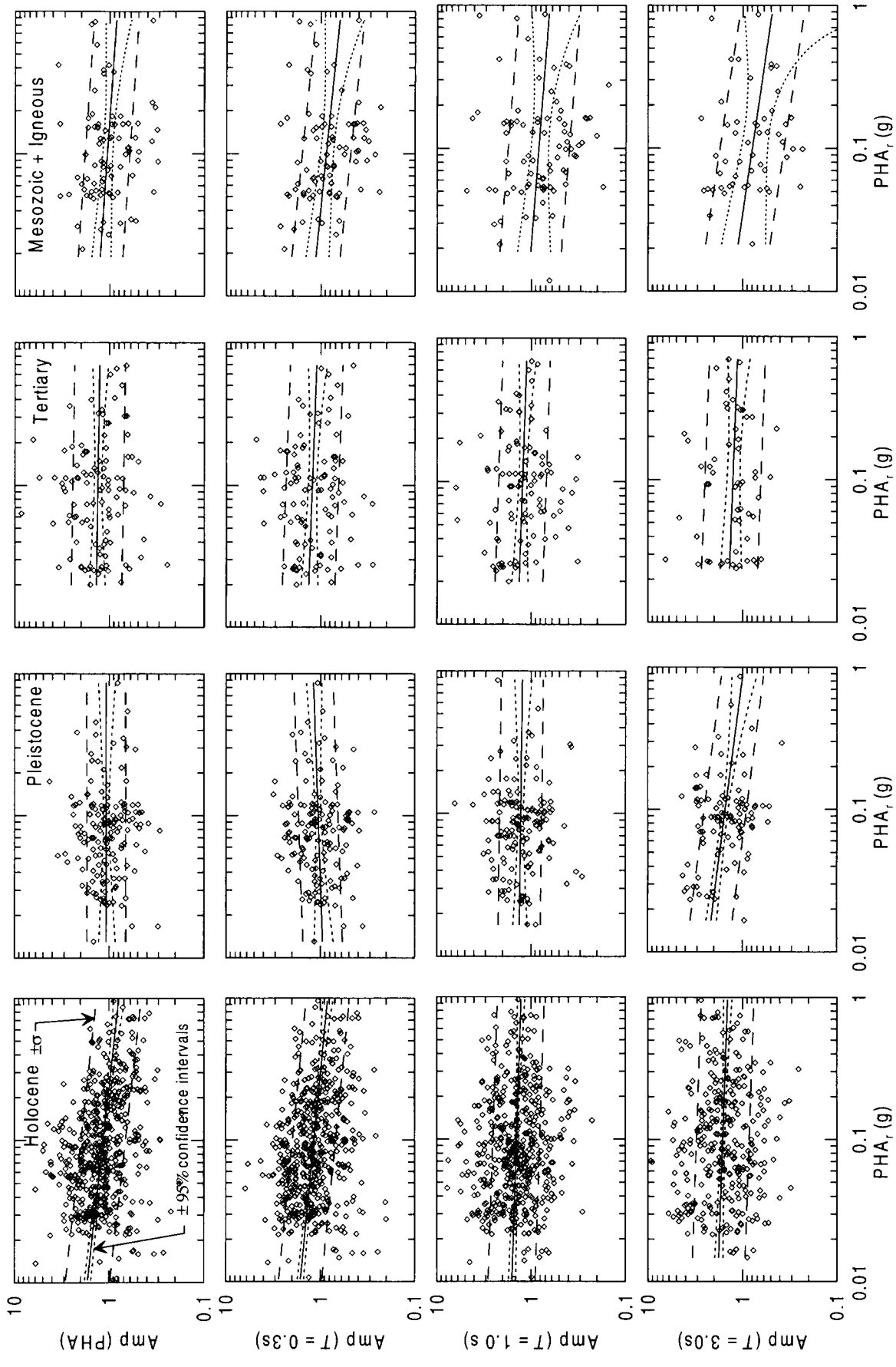

Figure 2. Spectral acceleration amplification factors for categories in age-only geologic classification scheme. PHA$_r$ refers to peak horizontal acceleration of reference motion.

Table 5
Regression Coefficients for S_a Amplification Factors, Age-Only Classification Scheme

Geology	Period	a	b	σ	Rejection Confidence for $b = 0$ Model (%)
Holocene (H)	PHA	−0.24 ± 0.14	−0.17 ± 0.05	0.54	100
	0.3 s	−0.18 ± 0.13	−0.15 ± 0.05	0.53	100
	1.0 s	0.24 ± 0.15	−0.05 ± 0.06	0.57	91
	3.0 s	0.36 ± 0.19	−0.05 ± 0.08	0.64	82
Pleistocene (P)	PHA	0.14 ± 0.27	0.02 ± 0.10	0.47	29
	0.3 s	0.22 ± 0.27	0.07 ± 0.10	0.48	80
	1.0 s	0.21 ± 0.32	−0.02 ± 0.12	0.52	23
	3.0 s	−0.03 ± 0.37	−0.19 ± 0.14	0.51	99
Tertiary (T)	PHA	0.23 ± 0.35	−0.02 ± 0.14	0.62	21
	0.3 s	0.09 ± 0.37	−0.05 ± 0.14	0.65	49
	1.0 s	0.09 ± 0.34	−0.05 ± 0.14	0.58	55
	3.0 s	0.10 ± 0.45	−0.06 ± 0.18	0.69	48
Mesozoic + Igneous (M + I)	PHA	−0.13 ± 0.30	−0.08 ± 0.12	0.52	78
	0.3 s	−0.46 ± 0.33	−0.14 ± 0.13	0.57	96
	1.0 s	−0.45 ± 0.46	−0.12 ± 0.19	0.75	78
	3.0 s	−0.74 ± 0.63	−0.22 ± 0.27	0.79	89

to the estimation error for b_i (both indicated in Table 5). When $|b_i|$ exceeds the estimation error, the nonlinearity is considered significant. Secondly, sample "t" statistics are compiled to test the null hypothesis that $b_i = 0$ and $a_i =$ overall data median. This statistical testing provides a significance level $= \alpha$ that the null hypothesis cannot be rejected. For clarity of expression, we tabulate in Table 5 values of $1 - \alpha$, which we refer to as a "rejection confidence for a b $= 0$ model." Large rejection confidence levels (i.e., >95%) suggest significant PHA_r-dependence in amplification factors.

The results in Table 5 indicate for Holocene sediments statistically significant PHA_r-dependence of amplification functions at small to intermediate periods (i.e., $T < \sim 1.0$ sec). At short periods (PHA, $T = 0.3$ sec), the rejection confidence for the b $= 0$ model is nearly 100%, and the estimated values of $|b_i|$ exceed their prediction errors. Amplification occurs for $PHA_r < 0.2g$, and deamplification occurs for $PHA_r > \sim 0.2g$. At longer periods ($T = 1.0$, 3.0 sec), the nonlinearity is less statistically significant and amplification occurs across the full range of PHA_r. Nonlinearity is generally not statistically significant for age categories other than Holocene.

A key issue when interpreting regression results for different site categories is the degree to which the data for different categories are distinct. This is evaluated using statistical F tests (Cook and Weiberg, 1999), which compare submodels with a full model. For example, a pair of submodels could be the regression results in Figure 2 and Table 5 for Holocene (H) and Pleistocene (P). The full model in this example would consist of a regression through all data in the H and P categories. The F test is performed by calculating the residual sum of squares (based on misfit from the median model prediction) for the submodels (RSS_1 and RSS_2) and the full model (RSS_f). Since RSS measures lack of fit, the submodels and full model are compared by examining the difference $RSS_f - (RSS_1 + RSS_2)$. If this difference is "small," then the submodels and full model fit the data about equally well. For well-populated submodel data spaces, this would imply that the submodels do not describe distinct data sets.

For normally distributed data sets, the F statistic is calculated as

$$F = \frac{(RSS_f - (RSS_1 + RSS_2))/((df_1 + df_2) - df_f)}{\hat{\sigma}^2}, \quad (5)$$

where df_i refers to the degree of freedom of regression fit i (two in this case), and

$$\hat{\sigma}^2 = \frac{RSS_1 + RSS_2}{N_f - (df_1 + df_2)}, \quad (6)$$

where $N_f =$ number of data points in the full model. This F statistic can be compared with the F distribution to evaluate a significance level (p) for the test. Large values of p (e.g., $p > 0.05$) are often taken to imply that the submodels are not distinct.

We compile the F statistic and significance level (p) for the category pairs of Holocene-Pleistocene, Pleistocene–Tertiary, and Tertiary–Mesozoic. These statistics are compiled in Table 6 for the geologic age-only classification scheme. We judge the distinction between categories to be significant for $p < 0.05$, moderate for $0.05 < p < 0.15$, and insignificant for $p > 0.15$.

Significantly distinct values of short period amplification factors (PHA and 0.3 sec) are observed between Holo-

Table 6
F-Statistics Indicating Distinction among Site Categories, Age-Only Classification Scheme

	PHA		T = 0.3 sec		T = 1.0 sec		T = 3.0 sec	
Categories	*F*	*p*	*F*	*p*	*F*	*p*	*F*	*p*
H-P	6.4	0.002	10.5	0.000	2.6	0.076	1.3	0.266
P-T	4.3	0.014	3.4	0.035	0.9	0.424	2.9	0.061
T-M+I	4.0	0.020	7.8	0.001	9.7	0.000	6.4	0.002

cene and Pleistocene sediments. Short period Pleistocene amplification is significantly distinct from Tertiary, which has larger amplification factors. Compilations of median borehole velocity profiles by geologic unit by Silva *et al.* (1999) suggest that the velocity gradient (i.e., increase of velocity with depth) in Tertiary sediments is greater than old alluvium (which we interpret as analogous to Pleistocene). This higher gradient may explain the larger short-period amplification factors in Tertiary. Medium- to long-period (T = 1.0 and 3.0 sec) amplification levels for Holocene–Pleistocene and Pleistocene–Tertiary sediments are moderately or insignificantly distinct. The Tertiary and Mesozoic + Igneous (M + I) categories (i.e., the categories encompassing the materials that would generally be considered "rock") have significantly distinct amplification levels at all periods, with T amplification exceeding M + I.

Results

Synthesis of Results for Each Classification Scheme

The data analysis procedures described in the previous section were repeated for data grouped according to the classification schemes listed in Tables 2–4. We identify here the distinct categories within each scheme that emerged from the analyses and discuss variations in the amplification factors across categories. Regression results for many individual periods are presented in the Appendix for recommended categories. Some minor adjustments to the coefficients have been made to smooth the variations between periods. Note that in some cases, non-zero b-values given in the appendix are not statistically significant, as discussed in the preceding section and further below.

Table 7 presents F statistics and significance levels (p) for category pairs associated with the detailed surface geology, NEHRP, and geotechnical data schemes. Table 8 presents regression results, standard error terms, and hypothesis test results for distinct categories. Regression results for recommended categories are plotted against data in Figures 3–6 for periods T = 0.3 and 1.0 sec (which were chosen to represent results at short- and mid-periods).

For the age + depositional environment geologic classification scheme, regression analyses were performed for the Holocene lacustrine/marine (Hlm), Holocene alluvium (Ha), Pleistocene alluvium (Pa), and Quaternary alluvium (Qa = Ha + Pa) categories. Regression analyses for other

Table 7
F-Statistics Indicating Distinction among Site Categories

	PHA		T = 0.3 sec		T = 1.0 sec		T = 3.0 sec	
Categories	*F*	*p*	*F*	*p*	*F*	*p*	*F*	*p*
Geology, Depositional Environment								
Hlm-Ha	6.2	0.002	1.2	0.293	2.1	0.119	2.0	0.138
Ha-Pa	0.9	0.421	3.0	0.052	0.7	0.504	0.3	0.731
Hlm-Qa	7.3	0.001	1.8	0.175	2.4	0.089	2.2	0.114
Qa-T	3.1	0.044	0.6	0.571	3.0	0.049	3.3	0.037
Geology, Material Texture								
Hc-Hm	6.5	0.002	3.7	0.025	2.1	0.121	2.1	0.121
Hc-Pc	0.7	0.499	0.1	0.886	0.7	0.499	0.6	0.561
Pc-Pm	0.2	0.851	0.3	0.748	2.9	0.061	0.3	0.756
Hm-Pm	3.6	0.028	1.1	0.328	1.7	0.178	1.2	0.308
NEHRP								
B-C	0.3	0.774	2.8	0.064	4.6	0.011	1.3	0.288
C-D	5.2	0.006	5.7	0.004	8.6	0.000	12.4	0.000
D-E	6.8	0.001	6.2	0.002	10.5	0.000	4.2	0.016
Geotechnical Data								
B-C	4.5	0.012	14.4	0.000	15.2	0.000	2.3	0.101
C-D	0.3	0.777	0.8	0.442	3.8	0.023	8.5	0.000
D-E	10.8	0.000	10.6	0.000	11.2	0.000	2.3	0.106

categories listed in Table 2 were not performed due to sparse data. The lack of distinction between Ha and Pa amplification levels shown in Table 7 motivated the use of the Qa category. Qa is significantly distinct from Hlm and Tertiary (T) for PHA, but the distinction is reduced at longer periods. Regression results for the Hlm and Qa categories are presented in Figure 3. Levels of amplification and nonlinearity in the Hlm category, which includes a significant number of sites from Imperial Valley and San Francisco bay–shore locations, are large at small periods and decrease gradually with increasing period. However, nonlinearity for Hlm is statistically significant across the full period range considered (T = 0.01–5 sec). Levels of nonlinearity in the Qa category are less than Hlm but are statistically significant.

For the age + material texture geologic classification scheme, regression analyses were performed within the Holocene and Pleistocene age groups for coarse and fine/mixed sediments (denoted Hc, Pc, Hm, and Pm). As shown in Table 7, Pleistocene categories Pc and Pm are insignificantly distinct at nearly all periods, and hence we considered subdivision of Pleistocene according to material texture to not be justified. The Hm category has significantly distinct variations from Hc at short period (PHA and 0.3 sec), but the subcategories are insignificantly distinct at longer periods ($T \geq$ 1.0 sec). Regression results for the Hm and Hc categories are presented in Figure 4 for periods of 0.3 and 1.0 sec. Category Hm exhibits higher levels of weak-motion amplification and short- to moderate-period nonlinearity than Hc.

Regression results for NEHRP categories B–E (defined in Table 3) are presented in Figure 5 for T = 0.3 and 1.0 sec. Regression analyses for Category A were not performed due to sparse data. The data are also fairly sparse for Categories B and E; thus the confidence intervals on the ampli-

Table 8
Regression Coefficients for Amplification Factors and Hypothesis Test Results

	PHA				0.3 sec				1.0 sec				3.0 sec			
Category	*a*	*b*	σ	Rej C.	*a*	*b*	σ	Rej C.	*a*	*b*	σ	Rej C.	*a*	*b*	σ	Rej C.
Hlm	−0.59	−0.39	0.47	100	−0.39	−0.25	0.44	100	0.02	−0.22	0.45	100	0.29	−0.19	0.48	98
Qa	−0.15	−0.13	0.52	100	−0.10	−0.11	0.51	100	0.20	−0.06	0.58	89	0.14	−0.14	0.65	99
Hc	−0.11	−0.10	0.52	96	−0.08	−0.08	0.53	90	0.13	−0.06	0.57	71	0.00	−0.17	0.64	97
Hm	−0.50	−0.33	0.51	100	−0.33	−0.24	0.46	100	0.10	−0.14	0.56	98	0.38	−0.09	0.55	80
NEHRP B	0.09	0.05	0.48	21	−0.16	0.08	0.44	33	−0.71	−0.13	0.78	32	−1.57	−0.54	0.36	99
NEHRP C	−0.06	−0.05	0.55	65	−0.22	−0.09	0.64	89	0.07	−0.03	0.74	36	−0.01	0.00	0.90	2
NEHRP D	0.08	−0.07	0.57	89	0.11	−0.04	0.54	68	0.38	−0.02	0.48	32	0.44	−0.01	0.55	16
NEHRP E	−0.60	−0.50	0.46	100	−0.49	−0.43	0.54	99	−0.24	−0.46	0.48	100	0.47	−0.18	0.46	77
Geot. B	0.07	0.07	0.55	51	−0.02	0.15	0.66	78	0.24	0.25	0.73	91	−0.41	−0.06	0.77	27
Geot. C	0.11	−0.04	0.60	51	−0.10	−0.12	0.62	97	0.04	−0.08	0.72	73	0.01	−0.03	0.83	28
Geot. D	−0.02	−0.08	0.56	94	0.08	−0.04	0.51	67	0.41	−0.01	0.49	21	0.42	−0.03	0.59	45
Geot. E	−0.82	−0.63	0.40	100	−0.89	−0.60	0.36	100	−0.27	−0.49	0.45	100	0.54	−0.13	0.48	64

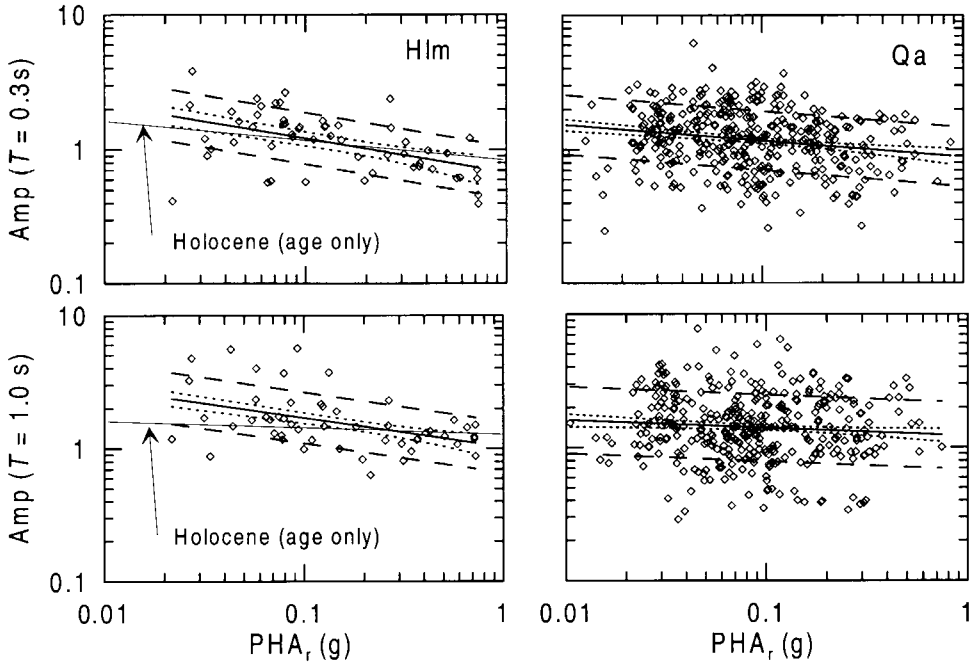

Figure 3. Spectral acceleration amplification factors for categories in the age + depositional environment classification scheme.

fication function are relatively wide. However, the results are considered sufficiently statistically robust to enable comparisons of amplification levels across site categories. Amplification levels for Categories B and C are not distinct for some individual periods (PHA, 3.0 sec), but are distinct at mid-periods (0.3, 1.0 sec) with C amplification exceeding B. The PHA_r-dependence of amplification in NEHRP B is generally statistically insignificant. For C, the PHA_r-dependence is moderate at short periods (PHA, 0.3 sec), and insignificant for $T > \sim 0.3$ sec. Amplification levels for NEHRP Categories C-D are significantly distinct at all periods, with the amplification being larger for NEHRP D than for C. The NEHRP D category has moderate nonlinearity at short periods (PHA, 0.3 sec) but has no significant nonlinearity for $T > \sim 0.3$ sec. Amplification levels for NEHRP Categories D-E are significantly distinct at all periods. Category E generally has the most significant PHA_r-dependence of amplification factors and the largest weak motion amplification. Nonlinearity for Category E has only moderate statistical significance for $T > 1.0$ sec. These trends for Category E are based on a small number of recordings (18) and are therefore tentative.

The amplification factors for NEHRP categories do not exactly match those for surface geology categories because there is not a one-to-one correspondence between $V_{s\text{-}30}$ and surface geology. NEHRP B amplification factors are gener-

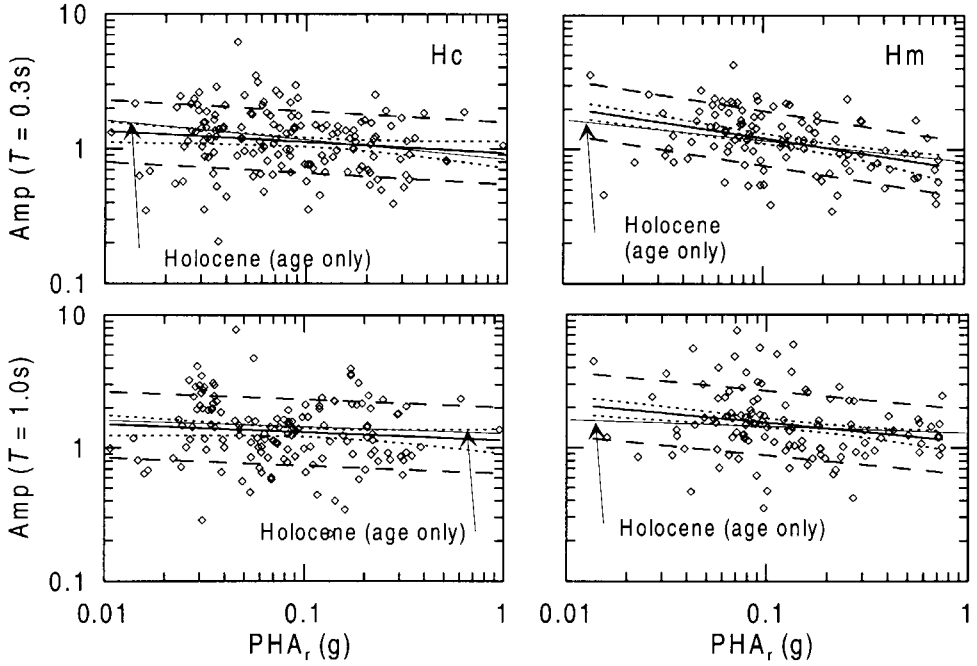

Figure 4. Spectral acceleration amplification factors for categories in the age + material texture classification scheme.

ally smaller than Mesozoic, which likely occurs because many of the Mesozoic geology sites in our database have $V_{s\text{-}30}$ smaller than the lower-bound NEHRP B threshold of 760 m/sec (e.g., among the 26 Mesozoic sites with NEHRP classifications, 13 are C, 10 are B, and 3 are A). The results for NEHRP C sites are generally intermediate between results for the geologic Pleistocene and Tertiary categories. Results for NEHRP D sites are generally intermediate between those for Holocene and Pleistocene sediments. Results for NEHRP E sites demonstrate more low-period nonlinearity and higher weak-motion amplification than any geologic category, including Hlm.

Regression results for Categories B–E in the Geotechnical Data classification scheme (Table 4) are presented in Figure 6. Regression analyses for Category A were not performed due to sparse data. Category B (intact rock) has substantial deamplification that is significantly distinct from Category C at low- to moderate-periods ($T \leq 1.0$ sec). Deamplification factors for B do not vary significantly with PHA_r, and are generally lower than those for the Mesozoic + Igneous category in the age-only geology classification scheme. For Categories C and D, short-period amplification levels ($T = 0.01$ and 0.3 sec) are not distinct, while intermediate to long-period amplification factors are significantly distinct with D exceeding C. This result is a reversal of trends discussed above in which intercategory distinction was generally greater at smaller period and may be associated with a sediment depth effect on long-period spectral ordinates (the geotechnical scheme is the only one that incorporates depth in the definition of the site categories, even though the depths considered in the scheme are much smaller than typical basin dimensions). The general levels of C and D amplification at small periods are comparable to those for Quaternary alluvial sediments. Nonlinearity is generally modest to weak in Categories C and D at small period ($T \leq 0.3$ sec) and weak at longer periods. Data for Category E indicate much larger weak-motion amplification and nonlinearity than C or D, however E nonlinearity is of only moderate statistical significance for $T > 1.0$ sec. As with the NEHRP E category, the trends for Geotechnical Category E are based on a small number of recordings (18) and are therefore tentative.

Comparison to Previous Studies

Several previous studies have developed amplification factors suitable for comparison to the results of this study. In Figure 7a–c we compare our results for geologic categories to those of Steidl (2000), which were derived using a non-reference site approach similar to that employed here (Steidl's amplification factors are derived relative to the Sadigh [1993] attenuation relationship for rock, which produces reference motions similar to those from Abrahamson and Silva [1997] attenuation [Abrahamson and Shedlock, 1997]). Our Qa amplification factors (Fig. 7a) are similar to those of Steidl for the Q (all Quaternary) and Qy (young Quaternary) categories. For Tertiary sites (Fig. 7b), our results indicate similar levels of amplification to those of Steidl, although a lower degree of short-period nonlinearity. For Mesozoic materials, our results show comparable overall amplification levels and degrees of apparent nonlinearity to those of Steidl. However, as noted previously, nonlinearity in the response of Mesozoic materials is not statistically sig-

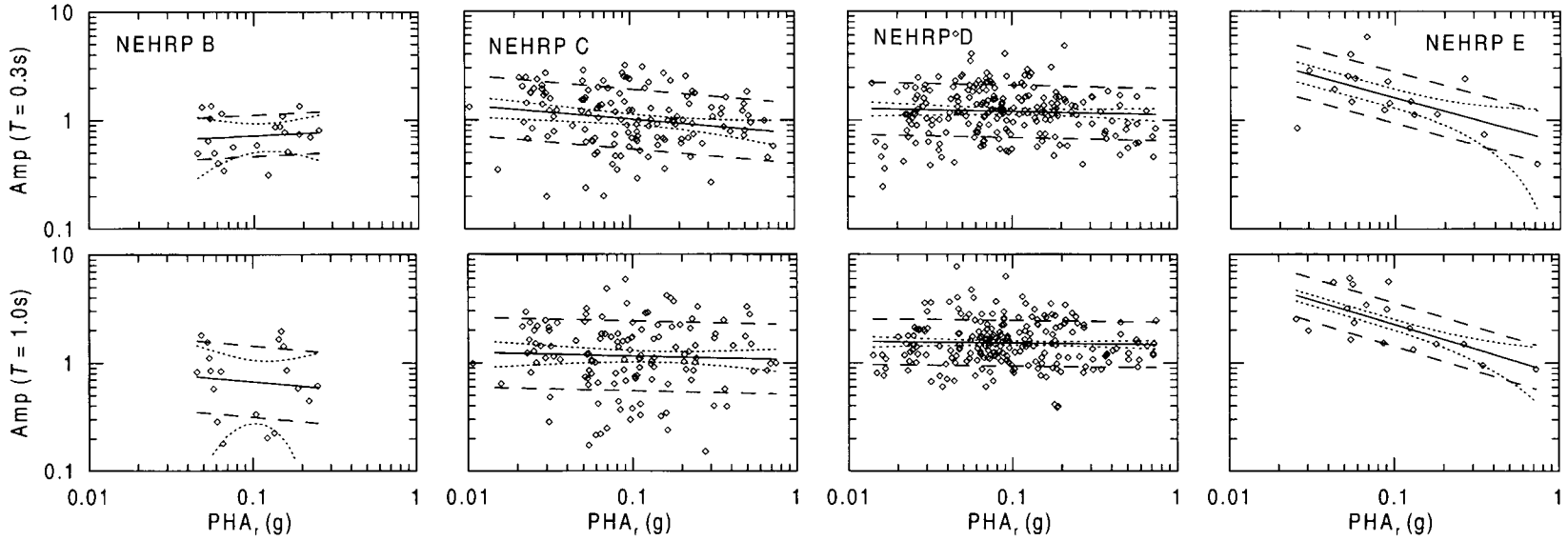

Figure 5. Spectral acceleration amplification factors for NEHRP Categories B-E.

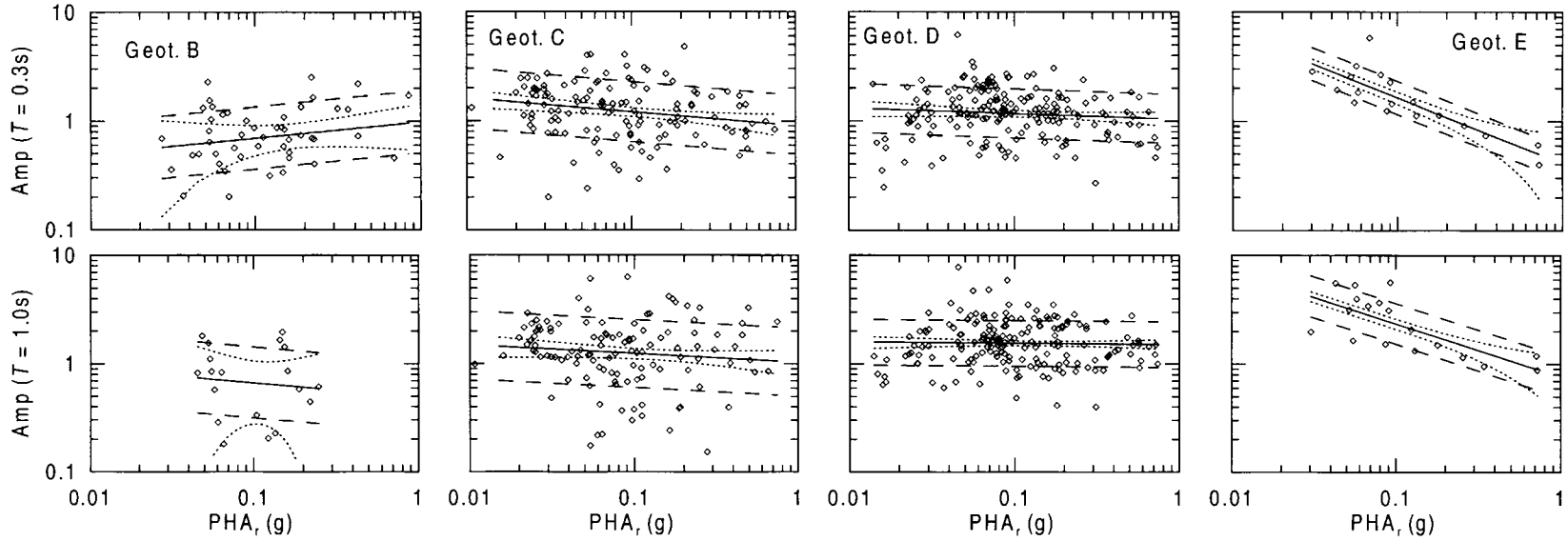

Figure 6. Spectral acceleration amplification factors for Geotechnical Categories B-E.

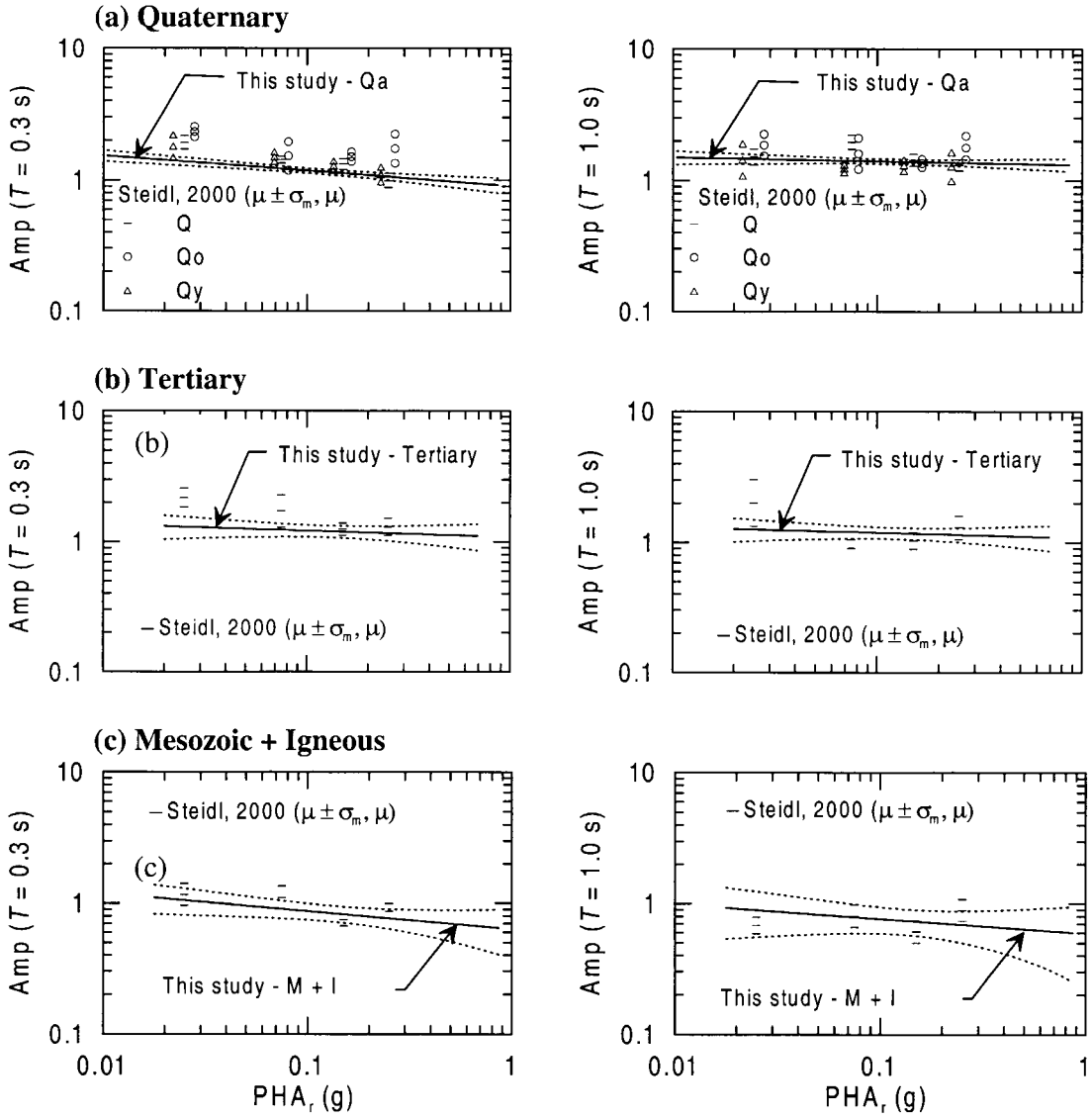

Figure 7. Comparison of results from this study and Steidl (2000) for (a) Quaternary alluvium, (b) Tertiary sediments, and (c) Mesozoic and Igneous geology. For Steidl's results, symbol μ denotes median, symbol σ_m denotes standard error of the median.

nificant because of the weak trend in the data relative to the large data scatter.

In Figure 8, we compare our results for NEHRP C and D sites to those of Borcherdt (2002), which were derived using a reference site approach with data from the 1994 Northridge earthquake. To facilitate the comparison, our results are presented for this figure in terms of averaged response spectral amplification levels across the period range of T = 0.1–0.5 sec (denoted F_a) and T = 0.5–2.0 sec (denoted F_v). Our results show lower amplification levels and less variation with PHA_r than was found by Borcherdt. One possible reason for the difference between our amplification levels and those of Borcherdt is different reference site conditions used in the derivation of amplification factors. We used a rock-average reference site condition for active regions (corresponding approximately to soft rock with $V_{s\text{-}30} \sim$ 520–620 m/sec), compared with a relatively competent reference rock condition used by Borcherdt ($V_{s\text{-}30} \sim$ 850 m/sec). The bias introduced by the different reference site conditions can be investigated with the $V_{s\text{-}30}$-based amplification factors of Borcherdt and Glassmoyer (1994) and Field (2000), which are linear (no dependence on PHA_r). The relative amplification between $V_{s\text{-}30}$ = 850 m/sec and about 570 m/sec represents the approximate bias that would be expected between our results and those of Borcherdt. Using the aforementioned references, these relative amplification values are approximately 1.15 for F_a and 1.3 for F_v. The average bias observed in Figure 8 (i.e., bias at $PHA_r \sim 0.1$g) for F_a is about 1.4, and for F_v is about 1.6. Accordingly, we attribute much of the difference between our amplification

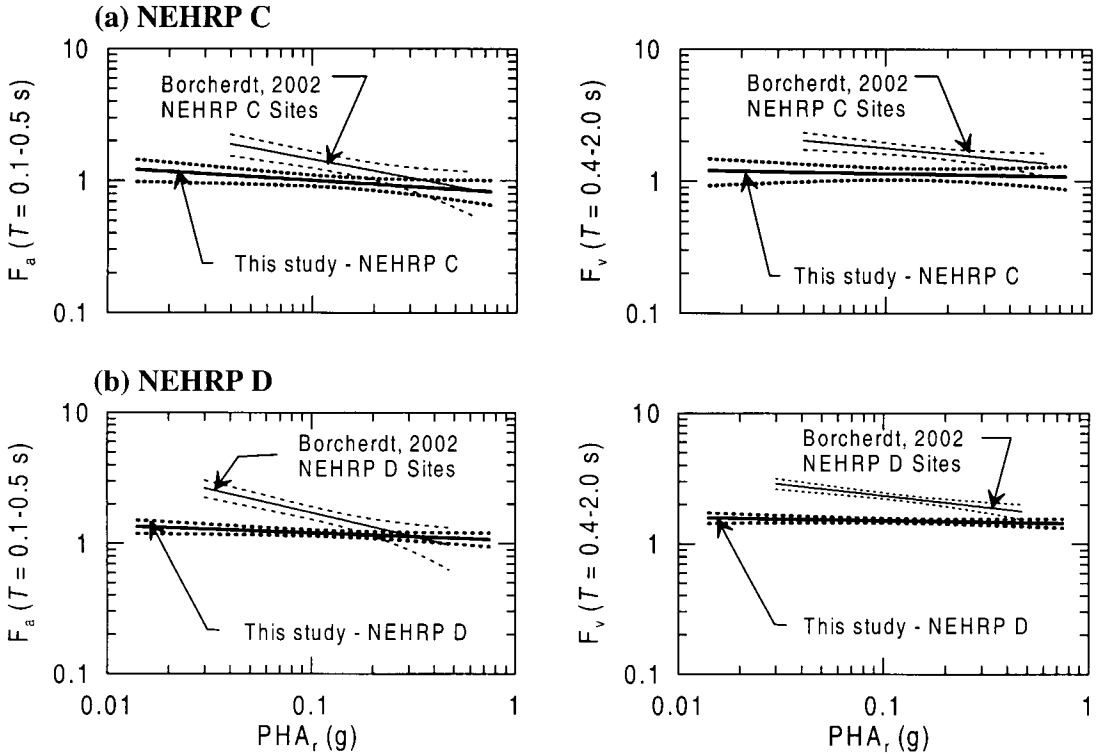

Figure 8. Comparison of results from this study to those of Borcherdt (2002).

factors and those of Borcherdt to the difference in reference site condition.

A third comparison is made between our surface geology-based (age + depositional environment) median amplification factors for $T = 0.3$ and 1.0 sec and the site terms in the Abrahamson and Silva (1997) attenuation relationship. These comparisons are shown in Figure 9a for soil categories and Figure 9b for rock categories. Note that the Abrahamson and Silva (A&S) site term is unity for rock. Our median amplification factors depart significantly from the A&S site terms for both rock categories (T and M + I) and for the Hlm soil category. Conversely, our amplification factors for Qa are very close to the A&S site term. Accordingly, use of the amplification factors from this study would have the greatest impact for geologic rock or soft soil site categories (or related categories from alternative classification schemes).

Magnitude- and Distance-Dependence of Results

In this section, we evaluate the magnitude and distance dependence of amplification factors and the magnitude-dependence of intra-category error terms. The regression equation used in the above analyses (equation 3a) is based on the assumption that amplification for a given site category is a function of only reference motion amplitude. Due to the finite time required for soil profiles to reach their steady-state resonant response, some dependence of amplification on the magnitude/duration of strong shaking might be expected. In Figure 10a we present residuals between individual amplification factors at $T = 0.3$ and 1.0 sec for Holocene sites and amplification-adjusted reference motions (using the regression results in Table 5). Also shown are the results of regression analyses performed according to:

$$\ln(\varepsilon_{ij}) = e_i + f_i\mathbf{M} + \tau_{ij}, \tag{7}$$

where e_i and f_i are regression coefficients for category i, **M** is moment magnitude, and τ_{ij} is an error term. The regression results indicate a magnitude-dependence in amplification factors at intermediate and long periods (e.g., $T \geq 1.0$ sec) but not at short periods (e.g., $T \leq 0.3$ sec). The standard error terms calculated from τ_{ij} at long periods are not reduced significantly from the values indicated in Table 5.

Plotted in Figure 10b are amplification-adjusted residuals for Holocene sites versus site-source distance. Also shown are linear regression analyses performed according to

$$\ln(\varepsilon_{ij}) = g_i + h_i \ln r + \gamma_{ij}, \tag{8}$$

where g_i and h_i are regression coefficients for category i, r = site-source distance (in kilometers), and γ_{ij} is an error term. No significant trend in the residuals with r is observed.

The variation of standard error term (σ) with magnitude and site category is shown in Figure 10c for age-only geologic categories, with the magnitude-dependent error terms from Abrahamson and Silva (1997) also shown for comparison. We find no significant magnitude-dependence in the

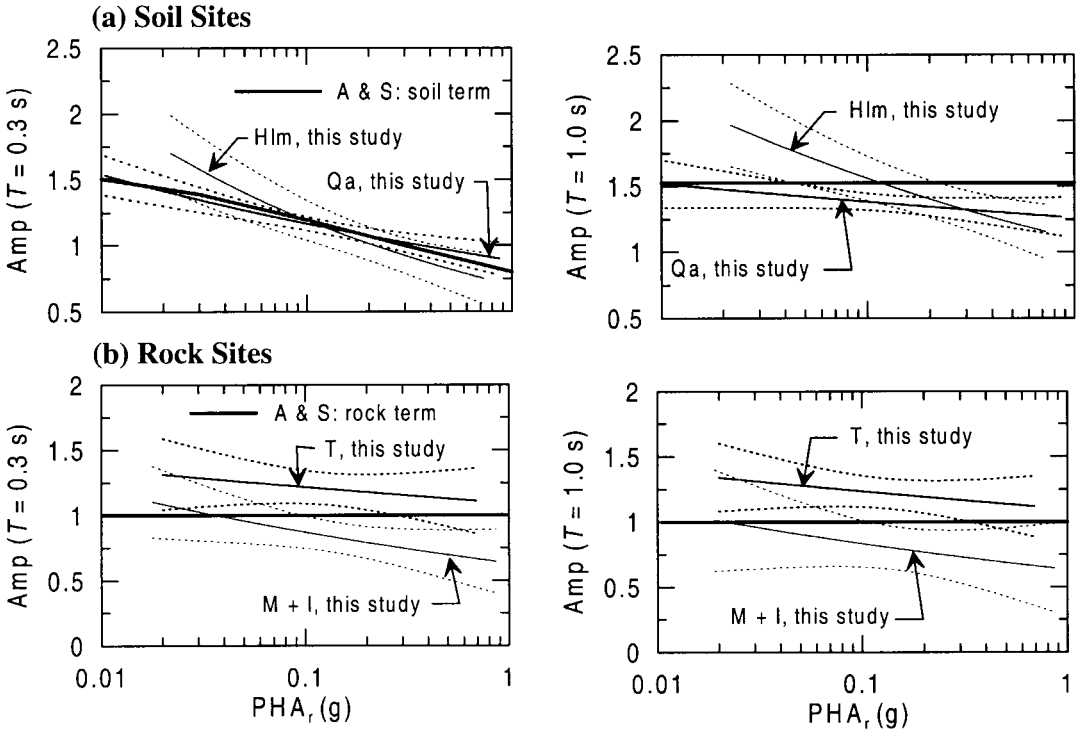

Figure 9. Comparison of median results for surface geology categories (this study) with site terms in Abrahamson and Silva (1997) attenuation relationship.

error terms but do find an increase of σ with period. The Abrahamson and Silva (1997) error terms decrease uniformly with magnitude for M 5–7 and also increase with period. Typically, error terms from this study are smaller than the Abrahamson and Silva terms for M <5.75 and larger for M >5.75.

Inter-Category Error Terms

One of the objectives of this research was to quantify the ability of different classification schemes to capture site-to-site variations of spectral acceleration. This is evaluated for a classification scheme using the inter-category standard error (σ_R), which is calculated as follows:

$$\sigma_R = \sqrt{\frac{\sum_{i=1}^{M_c}\sum_{i=1}^{N_i}(\varepsilon_{ij} - \varepsilon_i)^2}{(\sum_{i=1}^{M_c} N_i) - df}}, \quad (9)$$

where M_c = the number of categories in the scheme and df = total number of degrees-of-freedom in regression equations for the scheme ($df = 2 \times M_c$). Intercategory standard error σ_R represents the average dispersion of data within all categories belonging to a given scheme. This is calculated for five classification schemes, three of which are based on surface geology, one on near-surface shear-wave velocity ($V_{s\text{-}30}$), and one on geotechnical data.

Intercategory standard error terms for the soil and rock categories in each scheme are plotted as a function of period in Figures 11a and 11b, respectively. For soil categories (Fig. 11a), the largest error terms at all periods are obtained from the $V_{s\text{-}30}$-based and geotechnical classification schemes. The smallest error terms are generally from detailed geology schemes such as age + depositional environment or age + material texture. Maximum differences in the category dispersion values are as large as 0.1 in natural logarithmic units. These variations in dispersion are large enough to have an important effect on seismic hazard calculations (Field and Petersen, 2000). Also shown in Figure 11 for reference are the error terms from the Abrahamson and Silva (1997) attenuation relationship. Note that these error terms are strongly magnitude dependent, an effect that was not observed in this study (e.g., Fig. 10c).

For rock sites (Fig. 11b), the error terms are generally minimized at intermediate to long period ($T \geq 0.3$ sec) for the geology scheme (which is age-only for rock) and at short period (PHA) for the $V_{s\text{-}30}$-based scheme. The rock error terms for all schemes are larger than those for soil.

The data used to compile the inter-category error terms in Figure 11a,b include motions from all classified sites. These data sets are inconsistent to the extent that the various schemes have different numbers of classified sites. Accordingly, we compiled a list of 109 sites (with 187 recordings) for which classifications are available by all five of the categorization schemes considered herein. The inter-category error terms for this consistent data set are of a similar mag-

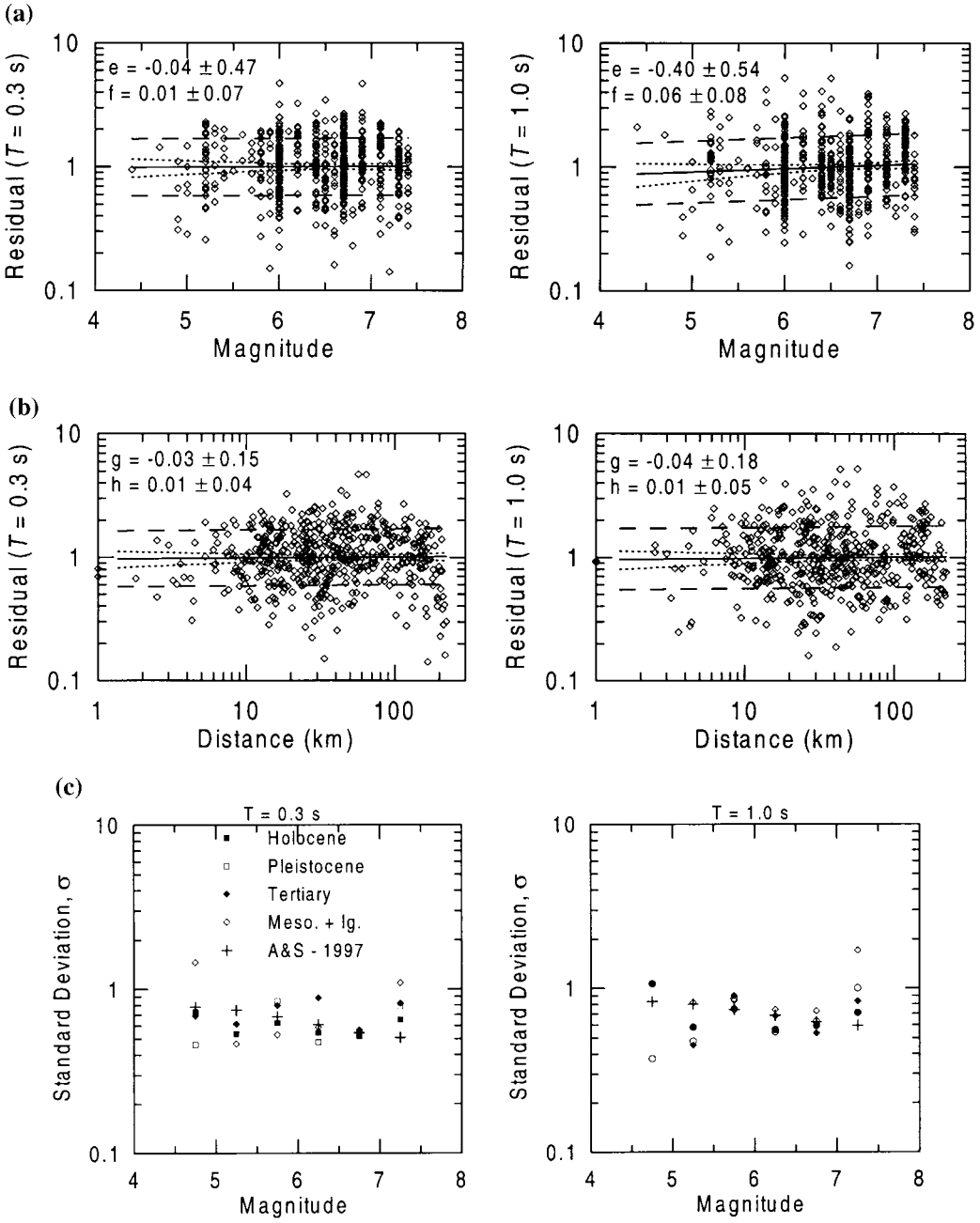

Figure 10. (a) Variation with magnitude of spectral acceleration residuals calculated using amplification-adjusted reference motions. Data are for Holocene soil sites. (b) Variation with site-source distance of spectral acceleration residuals calculated using amplification-adjusted reference motions. Data are for Holocene soil sites. (c) Variation of standard error term σ with magnitude and geologic age. Compare to magnitude-dependent term by Abrahamson and Silva (1997).

nitude and show similar trends to those for the full data set (Stewart *et al.*, 2001).

Conclusions and Recommendations

The identification of an "optimized" classification scheme for strong motion studies should consider two factors: (1) the degree to which amplification factors defined for categories within the scheme are capable of capturing site-to-site variations in ground motion, as measured by the dispersion of prediction residuals and (2) the degree to which amplification levels among categories within the various schemes are distinct from each other. With respect to the first criterion, our results suggest that for soil sites, ampli-

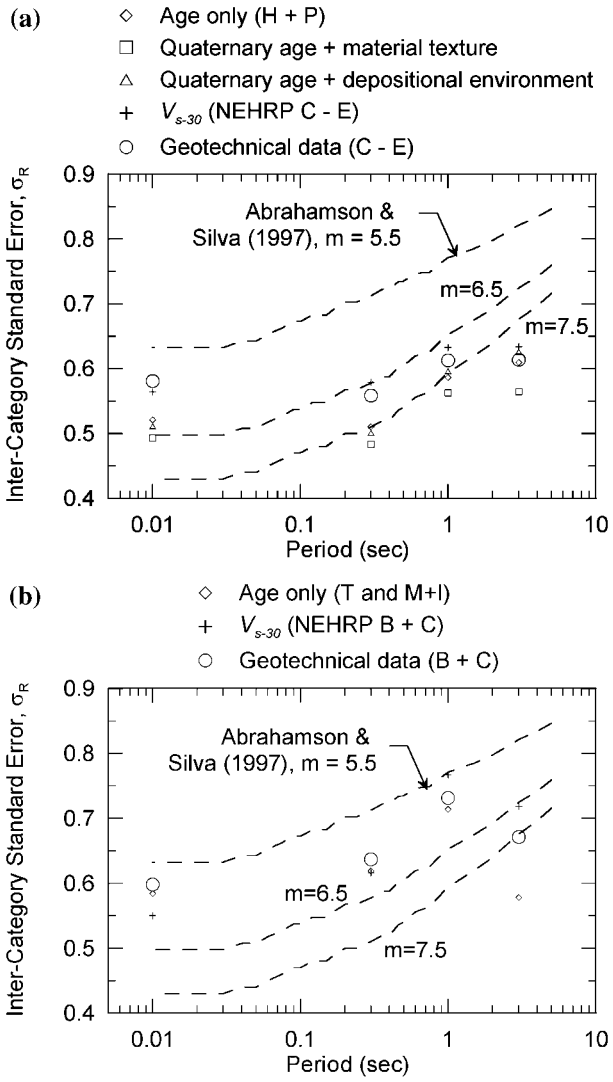

Figure 11. Intercategory standard error terms for spectral acceleration (this study) and error terms derived by Abrahamson and Silva (1997). Results apply for categories within the respective schemes associated with (a) young sediments (soil) and (b) soft rock and rock conditions.

fication factors defined for detailed surface geology classification schemes minimize the average dispersion of prediction residuals. Variations in dispersion between schemes are as large as 0.1 in natural logarithmic units, a difference that is sufficiently large to have an important effect on the results of hazard calculations (Field and Petersen, 2000). For rock sites, dispersion is minimized at short periods (PHA) with the use of the NEHRP scheme and at long periods ($T \geq 0.3$ sec) with the use of age-only surface geology. With respect to the second criterion, the NEHRP classification scheme (site categories distinguished on the basis of $V_{s\text{-}30}$) is the only one for which amplification levels between categories are generally distinct across a wide period range. At small periods, detailed surface geology categories also have distinct amplification levels.

Based on the results for soil sites, classification schemes based on detailed surface geology appear to provide an effective means by which to delineate site conditions for the evaluation of site amplification factors for short-period response spectral acceleration (e.g., PHA). The NEHRP scheme is also effective, particularly for evaluating amplification factors across a broad range of spectral periods. With regard to surface geology schemes, recommended categories for materials of Quaternary age are delineated on the basis of depositional environment or material texture as follows:

Depositional Environment	*Material Texture*
Quaternary alluvium	Holocene coarse-grained
Holocene lacustrine/marine	Holocene fine/mixed texture
	Pleistocene

For rock sites (i.e., pre-Quaternary materials), geologic classifications are based principally on age (i.e., the categories are T and M + I), and the dispersion of prediction residuals is relatively large. Future studies may be able to identify rock site categories defined on the basis of age + fracture spacing/degree-of-weathering that reduce the large dispersion at small periods. Lacking such data, however, the NEHRP classification scheme appears to provide an effective means of defining short-period amplification factors for rock sites.

At moderate to long periods ($T \geq 1.0$ sec), our results do not point to one scheme as being optimized with respect to the two criteria listed above. We speculate that this finding results in part from the fact that all of the classification schemes considered herein are based on features of relatively shallow geologic materials, which more significantly influence short-period components of ground motions than long-period components. Consideration of basin geometric parameters such as depth or distance to basin edge may be able to improve amplification models for soil sites, especially at long period. Recent work utilizing southern California data has been encouraging in this regard (Field, 2000; Joyner, 2000; Lee and Anderson, 2000; Steidl, 2000).

The results of this study can be applied to hazard analyses through a probability density function (PDF) that describes spectral acceleration conditional on site category as well as magnitude, distance, and other seismological variables. This PDF is usually log-normally distributed. The median of this distribution can be taken as the product of the median from a rock attenuation model and the applicable amplification factor. Rock attenuation models utilizing a database and regression approach similar to that of Abrahamson and Silva (1997) are considered appropriate for use with our amplification factors. Appropriate relations therefore include Abrahamson and Silva (1997), Sadigh *et al.* (1997), and Idriss (1991). The recommended amplification functions from this study are given by equation (3a) and the coefficients in the Appendix. The median amplification factors are significantly different from the Abrahamson and Silva site terms for rock categories (e.g., T, M + I) and soft

soil categories (e.g., Hlm). The standard error term (σ_{haz}) for the PDF can be taken as

$$\sigma_{haz} = \sqrt{\sigma^2 + 0.23^2}, \quad (10)$$

where σ is the appropriate category error term from this study. The additional error term of 0.23 accounts for inter-event variability, which was removed by use of the event term during the derivation of reference motions in this study. The value of 0.23 was obtained during the data regressions of Abrahamson and Silva (1997).

Acknowledgments

Support for this study was provided by the Pacific Earthquake Engineering Research Center through the Earthquake Engineering Research Centers Program of the National Science Foundation under Award Number EEC-9701568 and the California Department of Conservation, Division of Mines and Geology, Strong Motion Instrumentation Program, Contract 1098-712. This support is gratefully acknowledged. We thank Drs. Moh Huang and Anthony Shakal of CSMIP for their assistance in locating strong motion stations. We thank Charles Real of CDMG for his assistance in acquiring digital SCAMP maps. Bora Baturay, James Chen, and Steve Erickson of UCLA assisted with data synthesis and analysis. Dr. Roger Borcherdt of the USGS provided valuable advice and suggestions during numerous conversations on this topic.

References

Abrahamson, N. A. (2000). Effects of rupture directivity on probabilistic seismic hazard analysis, in *Proc. 6th Int. Conf. on Seismic Zonation*, Earthquake Engineering Research Institute, Oakland, California.

Abrahamson, N. A., and K. M. Shedlock (1997). Overview (of modern attenuation relationships), *Seism. Res. Lett.* **68,** no. 1, 9–23.

Abrahamson, N. A., and W. J. Silva (1997). Empirical response spectral attenuation relations for shallow crustal earthquakes, *Seism. Res. Lett.* **68(1),** 94–127.

Abrahamson, N. A. and R. R. Youngs (1992). A stable algorithm for regression analyses using the random effects model, *Bull. Seism. Soc. Am.* **82,** 505–510.

Anderson, J. G., M. D. Trifunac, T.-L. Teng, A. Amini, and K. Moslem (1981). Los Angeles vicinity strong motion accelerograph network, Report No. CE 81-04, University of Southern California, Los Angeles.

Ang, A.H.-S. and W. H. Tang (1975). *Probability Concepts in Engineering Planning and Design, Volume I*—Basic Principles, Wiley & Sons, New York.

Bazzuro, P. (1998). Probabilistic seismic demand analysis *Ph.D. Dissertation*, Civil Engineering Dept., Stanford University, Stanford, California.

Boatwright, J., L. C. Seekins, and C. S. Mueller (1991). Ground motion amplification in the Marina, *Bull. Seism. Soc. Am.* **81,** 1980–1997.

Boore, D. M., and L. T. Brown (1998). Comparing shear wave velocity profiles from inversion of surface wave phase velocities with down-hole measurements: systematic differences between the CXW method and down hole measurements at six USC strong motion sites, *Seism. Res. Lett.* **69,** 222–229.

Boore, D. M., W. B. Joyner, and T. E. Fumal (1997). Equations for estimating horizontal response spectra and peak acceleration from western North American earthquakes: A summary of recent work, *Seism. Res. Lett.* **68(1),** 128–153.

Borcherdt, R. D. (1994). Estimates of site-dependent response spectra for design (methodology and justification), *Earthquake Spectra* **10,** no. 4, 617–653.

Borcherdt, R. D. (2002). Empirical evidence for acceleration-dependent amplification factors, *Bull. Seism. Soc. Am.* **92,** 761–782.

Borcherdt, R. D., and G. Glassmoyer (1994). Influences of local geology on strong and weak ground motions recorded in the San Francisco Bay region and their implications for site-specific building-code provisions The Loma Prieta, California Earthquake of October 17, 1989—Strong Ground Motion, *U.S. Geol. Surv. Profess. Pap. 1551-A*, A77–A108

Campbell, K. W. (1997). Empirical near-source attenuation relations for horizontal and vertical components of peak ground acceleration, peak ground velocity, and pseudo-absolute acceleration response spectra, *Seism. Res. Lett.* **68(1),** 154–179.

Campbell, K. W. (2000). Erratum to Campbell, 1997, *Seism. Res. Lett.* **71,** no. 3, 352–354.

Campbell, K. W. (2001). Erratum to Campbell, 2000, *Seism. Res. Lett.* **72,** no. 4, 474.

Cook, R. D., and S. Weisberg (1999). *Applied Regression Including Computing and Graphics*, Wiley & Sons, New York.

Chang, S. W. (1996). Seismic response of deep stiff soil deposits, *Ph.D. Dissertation*, University of California, Berkeley.

Dickenson, S. E. (1994). The dynamic response of soft and deep cohesive soils during the Loma Prieta earthquake of October 17, 1989, *Ph.D. Dissertation*, University of California, Berkeley.

Earthquake Engineering Research Center (1995). Geotechnical reconnaissance of the effects of the January 17, 1995 Hyogoken-Nanbu earthquake, Japan, Report No. UCB/EERC-95/01, N. Sitar (Editor), University of California, Berkeley.

Field, E. H. (2000). A modified ground motion attenuation relationship for southern California that accounts for detailed site classification and a basin depth effect, *Bull. Seism. Soc. Am.* **90,** S209–S221.

Field, E. H. and K. H. Jacob (1995). A comparison and test of various site-response estimation techniques, including three that are not reference-site dependent, *Bull. Seism. Soc. Am.* **85,** 1127–1143.

Field, E. H., and M. D. Petersen (2000). "A test of various site-effect parameterizations in probabilistic seismic hazard analyses of Southern California," *Bull. Seism. Soc. Am.* **90,** S222–S244.

Fukushima, Y., K. Irikura, T. Uetake, and H. Matsumoto (2000). Characteristics of observed peak amplitude for strong ground motion from the 1995 Hyokoken Nanbu (Kobe) earthquake, *Bull. Seism. Soc. Am.* **90,** 545–565.

Fumal, T. E. (1978). Correlations between seismic wave velocities and physical properties of near-surface geologic materials in the southern San Francisco Bay region. California, *U.S. Geol. Sur. Open-File Report 78–1067* 114 pp.

Geomatrix Consultants (1993). Compilation of geotechnical data for strong motion stations in the Western United States, Report to Lawrence Livermore National Lab., Project No. 2256, Oakland, California.

Harmsen, S. C. (1997). Determination of site amplification in the Los Angeles urban area from inversion of strong motion records, *Bull. Seism. Soc. Am.* **87,** 866–887.

Hartzell, S. A., D. Carver, E. Cranswick, and A. Frankel (2000). Variability of site response in Seattle, Washington, *Bull. Seism. Soc. Am.* **90,** 1237–1250.

Idriss, I. M. (1991). "Procedures for selecting earthquake ground motions at rock sites," Report to U.S. Department of Commerce, Center for Geotechnical Modeling, University of California, Davis, revised 1993.

Joyner, W. B. (2000). Strong motion from surface waves in deep sedimentary basins, *Bull. Seism. Soc. Am.* **90,** S95–S112.

Lee, Y., and J. G. Anderson (2000). A custom southern California ground motion relationship based on analysis of residuals, *Bull. Seism. Soc. Am.* **90,** S170–S187.

Lee, C.-T., C.-T. Cheng, C.-W. Liao, and Y.-B. Tsai (2001). Site classification of Taiwan free-field strong motion stations, *Bull. Seism. Soc. Am.* **91,** 1283–1297.

Martin, G. M. (Editor) (1994). *Proceedings of the NCEER/SEAOC/BSSC Workshop on Site Response during Earthquakes and Seismic Code*

Provisions, University of Southern California, Los Angeles, 18–20 November 1992.

Morton, D. M., R. M. Hauser, and K. R. Ruppert (1999). Preliminary Digital Geologic Map of the Santa Ana 30′ × 60′ Quadrangle, Southern California, U.S. *Geol. Open-File Report 99–172.*

Rathje, E., I. M. Idriss, and P. Somerville (2000). Chapter 4: Strong ground motions and site effects, *Earthquake Spectra* **16,** Suppl. A, 65–96.

Rodriguez-Marek, A., J. D. Bray, and N. A. Abrahamson (2001). An empirical geotechnical seismic site response procedure, *Earthquake Spectra* **17,** no. 1, 65–87.

Rodriguez-Ordonez, J. A. (1994). A new method for interpretation of surface wave measurements in soils, *Ph.D. Dissertation*, North Carolina State University, Raleigh.

Sadigh, K. (1993). A review of attenuation relationships for rock site conditions from shallow crustal earthquakes in an interplate environment, in *Proc. Int. Workshop on Strong Motion Data* Menlo Park, California, Vol. 2, 179–236.

Sadigh, K., C.-Y. Chang, J. A. Egan, F. Makdisi, and R. R. Youngs (1997). Attenuation relations for shallow crustal earthquakes based on California strong motion data, *Seism. Res. Lett.* **68,** no. 1, 180–189.

Seed, H. B., and I. M. Idriss (1982) Ground motions and soil liquefaction during earthquakes Earthquake Engineering Research Institute Monograph Series, Vol. 5, Oakland, California.

Silva, W. J., N. Abrahamson, G. Toro, and C. Costantino (1997). Description and validation of the stochastic ground motion model, Report to Brookhaven National Laboratory, Associated Universities, Inc., Upton, New York.

Silva, W. J., S. Li, R. Darragh, and N. Gregor (1999). Surface geology based strong motion amplification factors for the San Francisco Bay and Los Angeles areas, Report to Pacific Earthquake Engineering Research Center, Pacific Engineering and Analysis, El Cerrito, California.

Shoja-Taheri, J. and J. G. Anderson (1988). The 1978 Tabas, Iran, earthquake: an interpretation of the strong motion records, *Bull. Seism. Soc. Am.* **78,** 142–171.

Sokolov, V. Y. (1997). Empirical models for estimating Fourier-amplitude spectra of ground acceleration in the northern Caucasus (Racha seismogenic zone), *Bull. Seism. Soc. Am.* **87,** 1401–1412.

Sokolov, V. Y., C.-H. Loh, and K.-L. Wen (2000). Empirical study of sediment-filled basin response: The case of Taipei City, *Earthquake Spectra* **16,** no. 3, 681–707.

Somerville, P. G., N. F. Smith, R. W. Graves, and N. A. Abrahamson (1997). Modification of empirical strong ground motion attenuation relations to include the amplitude and duration effects of rupture directivity, *Seism. Res. Lett.* **68,** 199–222.

Steidl, J. H. (2000). Site response in southern California for probabilistic seismic hazard analysis, *Bull. Seism. Soc. Am.* **90,** S149–S169.

Stewart, J. P. and A. H. Liu (2000). Ground motion amplification as a function of surface geology, in *Proc. SMIP2000 Seminar on Utilization of Strong Motion Data*, California Strong Motion Instrumentation Program, Sacramento, California, 1–22.

Stewart, J. P., A. H. Liu, Y. Choi, and M. B. Baturay (2001). Amplification factors for spectral acceleration in active regions, Report No. PEER-2001/10, Pacific Earthquake Engineering Research Center, University of California, Berkeley, (http://www.cee.ucla.edu/Faculty/jstewart/publications.htm).

Wills, C. J. and W. Silva (1998). "Shear wave velocity characteristics of geologic units in California," *Earthquake Spectra*, **14,** no. 3, 533–556.

Wills, C. J. M. Petersen, W. A. Bryant, M. Reichle, G. J. Saucedo, S. Tan, G. Taylor, and J. Treiman (2000). A site conditions map for California based on geology and shear wave velocity, *Bull. Seism. Soc. Am.* **90,** S187–S208.

Youngs, R. R. (1993). Soil amplification and vertical to horizontal ratios for analysis of strong motion data from active tectonic regions, Appendix 2C in *Guidelines for Determining Design Basis Ground Motions*, Vol. 2, Electrical Power Research Institute, Report No. TR-102293, Palo Alto, California.

Appendix

Smoothed Regression Coefficients and Standard Error Terms for Recommended Site Categories

(*Next two pages*)

Department of Civil and Environmental Engineering
5713 Boelter Hall
University of California, Los Angeles
Los Angeles, California 90095
(J.P.S., Y.C.)

Bechtel Corporation
50 Beale Street
P.O. Box 3965
San Francisco, California 94119
(A.L.)

Manuscript received 25 February 2002.

Table A1
Surface Geology Categories

Period	M+I			T			P			Hlm			Qa			Hc			Hm		
(sec)	*a*	*b*	σ	*a*	*b*	σ	*a*	*b*	σ	*a*	*b*	σ	*a*	*b*	σ	*a*	*b*	σ	*a*	*b*	σ
0.01	−0.13	−0.08	0.52	0.23	−0.02	0.62	0.14	0.02	0.47	−0.59	−0.39	0.47	−0.15	−0.13	0.52	−0.11	−0.10	0.52	−0.50	−0.33	0.51
0.02	−0.13	−0.08	0.52	0.17	−0.03	0.62	0.08	0.00	0.47	−0.55	−0.39	0.48	−0.14	−0.13	0.52	−0.10	−0.10	0.52	−0.48	−0.31	0.52
0.03	−0.11	−0.05	0.54	0.14	−0.03	0.63	0.03	0.00	0.48	−0.57	−0.36	0.49	−0.24	−0.14	0.52	−0.17	−0.10	0.52	−0.51	−0.29	0.52
0.04	−0.17	−0.03	0.56	−0.05	−0.03	0.64	−0.19	−0.02	0.48	−0.63	−0.33	0.50	−0.49	−0.14	0.51	−0.39	−0.10	0.53	−0.60	−0.29	0.52
0.05	−0.17	−0.02	0.55	−0.05	−0.04	0.66	−0.19	−0.01	0.47	−0.72	−0.34	0.47	−0.47	−0.13	0.51	−0.38	−0.09	0.53	−0.67	−0.27	0.50
0.06	−0.13	0.00	0.55	−0.05	−0.03	0.65	−0.19	−0.03	0.46	−0.70	−0.31	0.45	−0.46	−0.14	0.50	−0.36	−0.08	0.54	−0.66	−0.27	0.50
0.08	−0.11	−0.01	0.54	−0.05	−0.04	0.63	−0.20	−0.03	0.45	−0.70	−0.32	0.48	−0.43	−0.12	0.50	−0.29	−0.05	0.54	−0.66	−0.26	0.49
0.09	−0.10	−0.01	0.52	−0.05	−0.02	0.62	−0.09	0.01	0.45	−0.67	−0.31	0.52	−0.36	−0.11	0.51	−0.20	−0.01	0.55	−0.64	−0.25	0.49
0.10	−0.13	−0.02	0.51	−0.05	−0.03	0.61	−0.07	0.00	0.45	−0.67	−0.29	0.53	−0.35	−0.11	0.52	−0.18	−0.01	0.55	−0.62	−0.23	0.51
0.12	−0.16	−0.05	0.52	−0.05	−0.03	0.62	−0.05	0.01	0.45	−0.66	−0.30	0.54	−0.29	−0.10	0.53	−0.14	−0.03	0.55	−0.60	−0.23	0.52
0.15	−0.28	−0.11	0.54	−0.04	−0.03	0.62	−0.07	−0.01	0.46	−0.67	−0.33	0.54	−0.29	−0.12	0.53	−0.12	−0.04	0.54	−0.61	−0.27	0.52
0.17	−0.33	−0.12	0.55	−0.02	−0.05	0.63	−0.08	−0.03	0.46	−0.66	−0.33	0.54	−0.31	−0.14	0.52	−0.12	−0.05	0.54	−0.61	−0.29	0.52
0.20	−0.36	−0.12	0.56	−0.02	−0.06	0.64	−0.02	−0.01	0.47	−0.66	−0.32	0.52	−0.32	−0.15	0.52	−0.12	−0.08	0.54	−0.59	−0.28	0.51
0.24	−0.39	−0.14	0.56	0.00	−0.06	0.65	0.14	0.03	0.48	−0.49	−0.27	0.50	−0.20	−0.12	0.50	−0.11	−0.06	0.53	−0.47	−0.25	0.49
0.30	−0.40	−0.14	0.57	0.03	−0.05	0.65	0.22	0.07	0.48	−0.39	−0.25	0.48	−0.10	−0.11	0.51	−0.08	−0.08	0.53	−0.36	−0.24	0.47
0.36	−0.41	−0.12	0.65	0.04	−0.07	0.66	0.24	0.06	0.50	−0.26	−0.21	0.46	−0.02	−0.10	0.50	−0.01	−0.06	0.51	−0.27	−0.23	0.46
0.40	−0.44	−0.12	0.67	0.04	−0.06	0.66	0.25	0.06	0.50	−0.25	−0.22	0.46	0.00	−0.09	0.51	−0.01	−0.08	0.51	−0.23	−0.25	0.46
0.46	−0.46	−0.13	0.70	0.07	−0.05	0.64	0.25	0.02	0.52	−0.23	−0.21	0.46	0.04	−0.09	0.52	0.02	−0.08	0.51	−0.17	−0.23	0.48
0.50	−0.48	−0.14	0.71	0.07	−0.07	0.64	0.24	0.03	0.53	−0.17	−0.21	0.46	0.09	−0.08	0.53	0.04	−0.07	0.51	−0.10	−0.19	0.49
0.60	−0.55	−0.16	0.72	0.10	−0.07	0.63	0.27	0.03	0.53	−0.13	−0.23	0.49	0.12	−0.09	0.54	0.06	−0.08	0.53	0.00	−0.18	0.53
0.75	−0.53	−0.16	0.73	0.18	−0.03	0.64	0.27	0.03	0.53	−0.02	−0.21	0.49	0.09	−0.11	0.56	0.07	−0.09	0.55	0.05	−0.18	0.56
0.85	−0.44	−0.12	0.75	0.18	−0.02	0.65	0.25	−0.01	0.53	0.01	−0.21	0.48	0.10	−0.10	0.57	0.09	−0.07	0.56	0.07	−0.16	0.56
1.00	−0.45	−0.12	0.75	0.09	−0.05	0.58	0.21	−0.02	0.53	0.03	−0.22	0.45	0.20	−0.06	0.58	0.13	−0.06	0.57	0.10	−0.14	0.56
1.50	−0.47	−0.11	0.76	0.01	−0.04	0.63	−0.12	−0.18	0.52	0.08	−0.21	0.43	0.02	−0.14	0.61	−0.16	−0.18	0.61	0.14	−0.14	0.56
2.00	−0.72	−0.19	0.77	−0.07	−0.07	0.67	−0.21	−0.22	0.51	0.09	−0.22	0.49	−0.05	−0.18	0.63	−0.19	−0.20	0.63	0.18	−0.13	0.56
3.00	−0.74	−0.22	0.77	−0.08	−0.09	0.69	−0.30	−0.28	0.51	0.10	−0.23	0.48	−0.05	−0.19	0.66	−0.20	−0.21	0.67	0.23	−0.09	0.55
4.00	−0.75	−0.24	0.78	−0.09	−0.11	0.70	−0.40	−0.31	0.55	0.10	−0.24	0.48	−0.05	−0.20	0.68	−0.21	−0.23	0.72	0.25	−0.13	0.54
5.00	−0.75	−0.26	0.78	−0.10	−0.13	0.85	−0.40	−0.34	0.59	0.10	−0.25	0.48	−0.05	−0.21	0.69	−0.22	−0.25	0.78	0.28	−0.17	0.62

Table A2
NEHRP and Geotechnical Categories

Period	NEHRP B			NEHRP C			NEHRP D			NEHRP E			Geot. B			Geot. C			Geot. D			Geot. E		
(sec)	*a*	*b*	σ	*a*	*b*	σ	*a*	*b*	σ	*a*	*b*	σ	*a*	*b*	σ	*a*	*b*	σ	*a*	*b*	σ	*a*	*b*	σ
0.01	0.09	0.05	0.49	−0.06	−0.05	0.55	0.08	−0.07	0.57	−0.62	−0.52	0.48	0.07	0.07	0.56	0.11	−0.04	0.60	−0.02	−0.08	0.56	−0.82	−0.63	0.40
0.02	0.10	0.01	0.50	−0.07	−0.06	0.55	0.06	−0.07	0.57	−0.70	−0.51	0.48	0.09	0.07	0.56	0.10	−0.05	0.60	−0.03	−0.09	0.55	−0.75	−0.61	0.40
0.03	0.10	0.11	0.50	−0.12	−0.04	0.55	0.03	−0.06	0.56	−0.75	−0.51	0.49	0.05	0.09	0.56	0.07	−0.03	0.60	−0.07	−0.08	0.55	−0.74	−0.57	0.42
0.04	0.10	0.12	0.48	−0.31	−0.08	0.55	−0.17	−0.09	0.55	−0.81	−0.51	0.47	−0.05	0.08	0.56	−0.13	−0.07	0.60	−0.23	−0.09	0.53	−0.89	−0.56	0.40
0.05	0.16	0.18	0.45	−0.41	−0.09	0.55	−0.19	−0.07	0.54	−1.04	−0.54	0.44	−0.13	0.07	0.55	−0.18	−0.07	0.60	−0.28	−0.09	0.52	−0.99	−0.55	0.38
0.06	0.21	0.20	0.46	−0.40	−0.09	0.54	−0.20	−0.07	0.54	−1.05	−0.54	0.43	−0.13	0.06	0.55	−0.19	−0.08	0.60	−0.30	−0.08	0.51	−0.98	−0.55	0.38
0.08	0.19	0.17	0.45	−0.40	−0.11	0.54	−0.19	−0.07	0.55	−1.11	−0.54	0.43	−0.18	0.03	0.52	−0.18	−0.07	0.60	−0.30	−0.09	0.53	−1.14	−0.58	0.36
0.09	−0.07	0.06	0.42	−0.39	−0.08	0.55	−0.13	−0.05	0.56	−1.11	−0.54	0.44	−0.23	0.02	0.52	−0.15	−0.06	0.59	−0.23	−0.07	0.55	−1.12	−0.57	0.40
0.10	0.09	0.15	0.43	−0.38	−0.09	0.56	−0.12	−0.05	0.58	−1.05	−0.51	0.45	−0.22	0.02	0.53	−0.15	−0.06	0.60	−0.22	−0.07	0.56	−1.12	−0.54	0.40
0.12	0.16	0.17	0.44	−0.38	−0.10	0.55	−0.11	−0.04	0.58	−0.95	−0.46	0.46	−0.28	0.00	0.54	−0.16	−0.06	0.58	−0.17	−0.05	0.56	−1.12	−0.55	0.35
0.15	0.40	0.22	0.44	−0.38	−0.14	0.57	−0.10	−0.06	0.58	−0.74	−0.43	0.49	−0.19	0.01	0.57	−0.18	−0.11	0.58	−0.15	−0.06	0.55	−1.12	−0.57	0.36
0.17	0.30	0.22	0.46	−0.36	−0.13	0.58	−0.12	−0.10	0.56	−0.70	−0.43	0.50	−0.17	0.03	0.60	−0.24	−0.14	0.57	−0.12	−0.07	0.54	−1.14	−0.61	0.36
0.20	0.36	0.25	0.48	−0.35	−0.13	0.60	−0.12	−0.09	0.55	−0.63	−0.42	0.50	−0.14	0.04	0.62	−0.28	−0.15	0.57	−0.09	−0.05	0.54	−1.08	−0.59	0.36
0.24	0.05	0.16	0.47	−0.30	−0.12	0.61	−0.02	−0.07	0.54	−0.55	−0.41	0.52	−0.10	0.08	0.65	−0.23	−0.15	0.58	−0.02	−0.05	0.52	−0.89	−0.56	0.32
0.30	−0.06	0.08	0.45	−0.22	−0.09	0.64	0.11	−0.04	0.54	−0.45	−0.41	0.54	−0.04	0.15	0.70	−0.10	−0.12	0.62	0.08	−0.04	0.51	−0.83	−0.55	0.36
0.36	−0.12	0.15	0.58	−0.19	−0.09	0.67	0.15	−0.03	0.53	−0.41	−0.40	0.53	−0.02	0.17	0.76	−0.02	−0.11	0.64	0.12	−0.04	0.50	−0.79	−0.54	0.37
0.40	−0.16	0.11	0.61	−0.14	−0.07	0.70	0.16	−0.04	0.51	−0.40	−0.40	0.54	0.00	0.19	0.75	0.01	−0.09	0.65	0.13	−0.04	0.49	−0.78	−0.53	0.39
0.46	−0.30	0.03	0.63	−0.11	−0.07	0.70	0.20	−0.07	0.49	−0.36	−0.40	0.54	0.01	0.18	0.75	0.04	−0.09	0.66	0.18	−0.06	0.48	−0.70	−0.52	0.44
0.50	−0.37	0.00	0.65	−0.07	−0.06	0.70	0.26	−0.04	0.49	−0.31	−0.40	0.54	0.02	0.19	0.76	0.09	−0.07	0.66	0.20	−0.05	0.49	−0.57	−0.52	0.47
0.60	−0.46	−0.02	0.67	−0.06	−0.07	0.72	0.30	−0.03	0.51	−0.25	−0.40	0.50	0.02	0.16	0.75	0.12	−0.06	0.68	0.24	−0.06	0.49	−0.30	−0.48	0.48
0.75	−0.65	−0.14	0.70	0.02	−0.06	0.72	0.40	−0.01	0.49	−0.18	−0.40	0.46	0.06	0.15	0.74	0.15	−0.05	0.70	0.36	−0.03	0.49	−0.20	−0.46	0.45
0.85	−0.70	−0.13	0.77	0.04	−0.05	0.73	0.39	−0.01	0.49	−0.12	−0.39	0.44	0.15	0.20	0.74	0.11	−0.06	0.71	0.38	−0.02	0.49	−0.18	−0.45	0.40
1.00	−0.72	−0.13	0.78	0.07	−0.03	0.74	0.38	−0.02	0.48	−0.09	−0.39	0.47	0.24	0.25	0.73	0.04	−0.08	0.72	0.41	−0.01	0.49	−0.12	−0.42	0.45
1.50	−0.88	−0.27	0.57	0.04	−0.03	0.77	0.34	−0.04	0.50	−0.02	−0.38	0.48	0.19	0.21	0.70	−0.06	−0.09	0.75	0.42	−0.03	0.51	0.07	−0.33	0.45
2.00	−1.33	−0.43	0.47	−0.01	−0.04	0.80	0.27	−0.07	0.51	0.03	−0.37	0.48	−0.41	−0.01	0.68	−0.12	−0.09	0.76	0.33	−0.05	0.55	0.14	−0.29	0.45
3.00	−1.47	−0.50	0.36	−0.08	−0.07	0.87	0.27	−0.09	0.55	0.09	−0.35	0.49	−0.44	−0.08	0.77	−0.12	−0.10	0.79	0.22	−0.10	0.59	0.25	−0.18	0.45
4.00	−1.55	−0.52	0.33	−0.20	−0.09	0.92	0.27	−0.09	0.57	0.10	−0.32	0.50	−0.47	−0.11	0.82	−0.12	−0.10	0.83	0.15	−0.14	0.65	0.30	−0.15	0.45
5.00	−1.60	−0.54	0.37	−0.25	−0.10	1.04	0.27	−0.10	0.66	0.12	−0.31	0.50	−0.50	−0.15	0.94	−0.12	−0.10	0.99	0.10	−0.16	0.71	0.33	−0.10	0.45